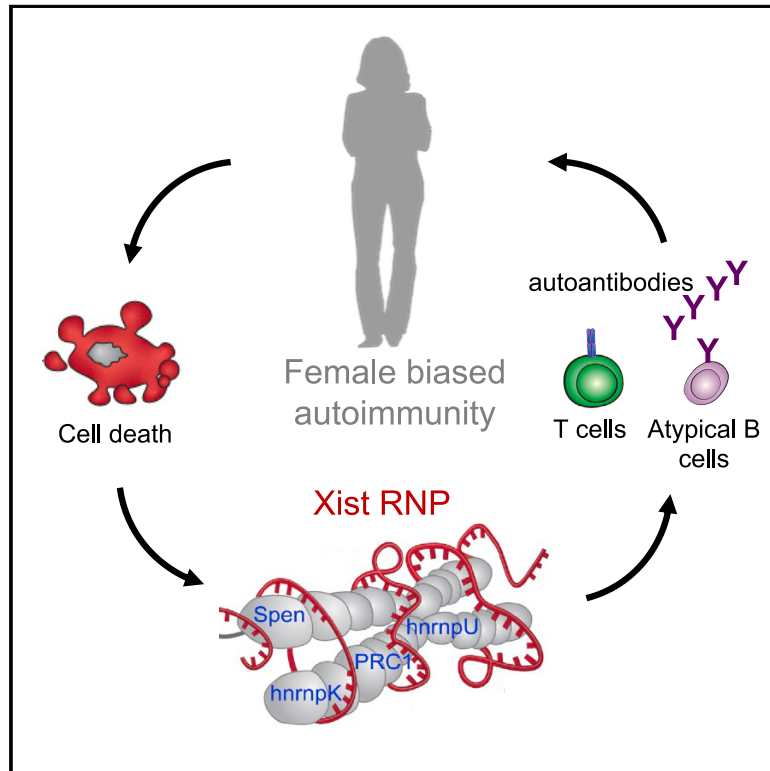


# Xist ribonucleoproteins promote female sex-biased autoimmunity

## Graphical abstract



## Authors

Diana R. Dou, Yanding Zhao, Julia A. Belk, ..., Anton Wutz, Paul J. Utz, Howard Y. Chang

## Correspondence

howchang@stanford.edu

## In brief

The Xist RNA protein complex, present only in females, is immunogenic and may underlie female-biased autoimmunity.

## Highlights

- Transgenic mouse models inducibly express Xist in male animals
- Xist expression in males induces autoantibodies and autoimmune pathology
- Xist in males reprograms T and B cell populations to female-like patterns
- Autoantibodies to Xist RNP characterize female-biased autoimmune diseases in patients



## Article

# Xist ribonucleoproteins promote female sex-biased autoimmunity

Diana R. Dou,<sup>1</sup> Yanding Zhao,<sup>1</sup> Julia A. Belk,<sup>1</sup> Yang Zhao,<sup>1</sup> Kerriann M. Casey,<sup>2</sup> Derek C. Chen,<sup>1</sup> Rui Li,<sup>1</sup> Bingfei Yu,<sup>1</sup> Suhas Srinivasan,<sup>1</sup> Brian T. Abe,<sup>1</sup> Katerina Kraft,<sup>1</sup> Ceke Hellström,<sup>3</sup> Ronald Sjöberg,<sup>3</sup> Sarah Chang,<sup>4</sup> Allan Feng,<sup>4</sup> Daniel W. Goldman,<sup>5</sup> Ami A. Shah,<sup>5</sup> Michelle Petri,<sup>5</sup> Lorinda S. Chung,<sup>4</sup> David F. Fiorentino,<sup>6</sup> Emma K. Lundberg,<sup>7,8</sup> Anton Wutz,<sup>9</sup> Paul J. Utz,<sup>4,10</sup> and Howard Y. Chang<sup>1,11,12,\*</sup>

<sup>1</sup>Center for Personal Dynamic Regulomes, Program in Epithelial Biology, Department of Dermatology, Stanford University School of Medicine, Stanford, CA, USA

<sup>2</sup>Department of Comparative Medicine, Stanford University, Stanford, CA, USA

<sup>3</sup>Autoimmunity and Serology Profiling, Division of Affinity Proteomics, Department of Protein Science, KTH Royal Institute of Technology, SciLifeLab, Stockholm, Sweden

<sup>4</sup>Department of Medicine, Division of Immunology and Rheumatology, Stanford University School of Medicine, Stanford, CA, USA

<sup>5</sup>Department of Medicine, Division of Rheumatology, Johns Hopkins University School of Medicine, Baltimore, MD, USA

<sup>6</sup>Department of Dermatology, Stanford University School of Medicine, Redwood City, CA, USA

<sup>7</sup>School of Engineering Sciences in Chemistry, Biotechnology and Health, KTH Royal Institute of Technology, SciLifeLab, Stockholm, Sweden

<sup>8</sup>Departments of Bioengineering and Pathology, Stanford University, Stanford, CA, USA

<sup>9</sup>Department of Biology, Institute of Molecular Health Sciences, Swiss Federal Institute of Technology, ETH Hönggerberg, Zurich, Switzerland

<sup>10</sup>Institute for Immunity, Transplantation and Infection, Stanford University School of Medicine, Stanford, CA, USA

<sup>11</sup>Howard Hughes Medical Institute, Stanford University, Stanford, CA 94305, USA

<sup>12</sup>Lead contact

\*Correspondence: [howchang@stanford.edu](mailto:howchang@stanford.edu)

<https://doi.org/10.1016/j.cell.2023.12.037>

## SUMMARY

Autoimmune diseases disproportionately affect females more than males. The XX sex chromosome complement is strongly associated with susceptibility to autoimmunity. Xist long non-coding RNA (lncRNA) is expressed only in females to randomly inactivate one of the two X chromosomes to achieve gene dosage compensation. Here, we show that the Xist ribonucleoprotein (RNP) complex comprising numerous autoantigenic components is an important driver of sex-biased autoimmunity. Inducible transgenic expression of a non-silencing form of Xist in male mice introduced Xist RNP complexes and sufficed to produce autoantibodies. Male SJL/J mice expressing transgenic Xist developed more severe multi-organ pathology in a pristane-induced lupus model than wild-type males. Xist expression in males reprogrammed T and B cell populations and chromatin states to more resemble wild-type females. Human patients with autoimmune diseases displayed significant autoantibodies to multiple components of XIST RNP. Thus, a sex-specific lncRNA scaffolds ubiquitous RNP components to drive sex-biased immunity.

## INTRODUCTION

Autoimmune diseases are the third most prevalent disease category, outpaced only by cancer and heart disease.<sup>1</sup> Four out of five patients with autoimmune diseases are female. For instance, in systemic lupus erythematosus (SLE), the ratio of patient sex is 9:1 females to males; the ratio in Sjögren's disease is 19:1 female to male patients.<sup>2,3</sup> Although hormones have been extensively studied,<sup>4</sup> the dosage of X chromosome appears to be a major driver of autoimmune risk irrespective of sex or hormonal status in humans and mice.<sup>5–8</sup> Patients with Klinefelter syndrome (XXY) are phenotypically males, have male hormonal pattern, but have an elevated risk of autoimmune disease equivalent to females. Specific X-linked genes, such as *TLR7*, that can escape X inactivation

have been nominated as contributors to specific autoimmune diseases.<sup>5–8</sup> The genetic risk underlying autoimmune diseases from the second X chromosome in aggregate remains unresolved. In addition, identical twin studies have also shown varying degrees of autoimmune disease penetrance, suggesting a genetic disposition that is also reliant on environmental factors.<sup>9,10</sup> Hence, adjuvant triggers<sup>11</sup> in addition to genetic predisposition may be initiators of autoimmune disease development.

Mammalian females have a XX genotype and males have a XY genotype. To make the gene expression output roughly equivalent between females and males, every cell in a female's body epigenetically silences one of two X chromosomes via the action of the long non-coding RNA (lncRNA) Xist. Xist is an ~17-kb lncRNA (19 kb in human) that is transcribed only from the inactive



X chromosome and thus not expressed in males. Xist is critical for the establishment of X chromosome inactivation (XCI) spreading from the X-inactivation center and coating the entire inactive X in association with its protein partners. During XCI establishment in mouse embryonic stem cells, Xist associates with 81 unique binding proteins to form an ribonucleoprotein (RNP) complex, 10 through direct RNA protein interaction and others through indirect protein-protein interaction.<sup>12,13</sup> Xist is widely expressed in adult somatic tissues and associates with additional tissue-specific proteins.<sup>14</sup> Several Xist binding proteins were previously noted to be autoantigens.<sup>12</sup> Studies in SLE patients and mice demonstrated that DNA-autoantibody and RNA-autoantigen immune complexes, such as Sm/RNP and U1A, activate the TLR7, TLR8, and TLR9 pathways of the innate immune system.<sup>15–17</sup> The XIST RNP, which comprised an lncRNA, bound RNA binding proteins, and tethered to pieces of genomic DNA, presents qualities resembling nucleic acid-autoantigen immune complexes.

To study the impact of the XIST RNP in autoimmune predilection independent of sex chromosome or hormonal background, we utilized an inducible and non-silencing allele of *Xist* introduced into an autosome in the autoimmune-resistant C57BL/6J and autoimmune-prone SJL/J strain backgrounds. Inducing transgenic Xist RNP formation in male animals allowed the study of this female-specific lncRNA in a male background, using a chemically induced SLE model. Both increased disease severity and elevated autoreactive lymphocyte pathway signatures were observed in the mouse models of pristane-induced SLE. Concurrently, we designed an antigen array to test autoimmune patient seroactivity to XIST-associating proteins and detected significant reactivity toward multiple components of the XIST RNP. Altogether, our data point to a significant role for the Xist RNP as a driver for autoimmunity that may underly the sex-biased female preponderance for developing autoimmune diseases.

## RESULTS

### Xist RNPs as autoantigens in human disease

A defining feature of many autoimmune diseases is the development of antibodies against self-proteins, termed autoantibodies. Many autoantibodies are directed toward nuclear RNA binding proteins, and the nature and titer of such autoantibodies define the type and severity of autoimmune diseases in clinical practice. We and others have identified the constellation of RNA binding proteins associated with Xist RNA in several cell types.<sup>12–14</sup> Bibliomic analysis revealed that 30 proteins of Xist RNP constituents have been reported as the targets of autoantibodies (i.e., autoantigens) in one or more human diseases (Figure S1; Table S1). This observation stimulated the hypothesis that Xist RNP may promote female-biased autoimmunity.

### Developing the TetOP- $\Delta$ RepA-Xist transgenic mouse to model autoimmune diseases

To test Xist RNP as a potential trigger of autoimmunity, we developed a TetOP- $\Delta$ RepA-Xist transgenic mouse that enables inducible expression of *Xist* in male animals. Because Xist expression from an autosome silences the chromosome in *cis* and is often cell lethal, we chose to use  $\Delta$ RepA-Xist, a truncation

of Xist that removes the A-repeat (RepA) element required for gene silencing activity of Xist,<sup>18</sup> but it does not ablate chromosome coating or Xist RNP formation. Previous study indicated that 78 of 81 proteins in the Xist RNP associates with  $\Delta$ RepA-Xist.<sup>12</sup> Expression of the  $\Delta$ RepA mutant Xist is controlled through the Tet-operon promoter (TetOP), and the transgenic cassette is inserted in the *Col1A1* locus on chromosome 11 (Figure 1A). Since Xist is expressed on only one of the two X chromosomes, we used mice heterozygous for TetOP- $\Delta$ RepA-Xist (denoted as tgXist onward) in our studies. After only 2 weeks of doxycycline (Dox) administration in heterozygous tgXist male mice, expression of *tgXist* was detectable through Xist quantitative reverse-transcription PCR (RT-qPCR) in multiple tissues and as single-punctate foci in the nucleus reminiscent of Barr body, as evidenced by RNA fluorescence *in situ* hybridization (FISH) (Figures 1B and 1C). We note that in the absence of induction, tgXist has a low level of expression that is detectable by RT-qPCR and by FISH; upon induction, tgXist level increases  $\sim$ 100-fold to approximate the level of endogenous Xist in female tissues (Figures 1B–1D). tgXist did not reduce chromatin accessibility or RNA expression locally at the locus of transgene insertion or across chromosome 11 (Figures S2A–S2D), consistent with the notion that  $\Delta$ RepA-Xist is functionally null for gene silencing.<sup>19</sup> Backcrossing of the inducible tgXist transgene into common mouse strains enables the study of *Xist* in male animals in multiple autoimmune disease models.

### Effect of genetic background on tgXist and autoimmunity

The pristane model of SLE has a well-documented female bias in disease penetrance and severity in the permissive SJL/J genetic background. In contrast, C57BL/6J mice,<sup>20,21</sup> the most widely used genetic background, are autoimmune resistant, and male mice are not expected to develop pristane-induced SLE.<sup>20</sup> The level at which pristane-induced phenotypes are halted is unclear. We first tested the effect of tgXist expressing on surrogate markers of autoimmunity to understand whether the *tgXist* transgene changed the requirement for genetic background in this mouse model of autoimmunity. Male and female C57BL/6J mice heterozygous for the  $\Delta$ RepA-Xist transgene were injected with pristane to chemically induce SLE<sup>20,22–24</sup> and evaluated for disease (Figure 1E). The pristane-injected transgenic cohorts consisted of a female control untreated for Dox (female), male control untreated for Dox (tg male), and the test group of male mice continuously treated with Dox to induce *tgXist* expression (male + Dox) (Figure 1F). Pristane-treated and untreated wild-type (WT) males of the same background were included as additional WT male controls. The rationale for each treatment cohort and comparison control is detailed in Table S2.

We found that pristane-treated tgXist male mice in C57BL/6J background do not exhibit disease even after 1 year, which is three times the duration for severe disease induction in SJL/J background (16 weeks). While tgXist mice developed anti-nuclear antibodies (ANAb), none of the specific autoantibodies examined were significantly different between tgXist male + pristane vs. WT male + pristane mice of the same age (Figures S3A and S3B). A subset of the tgXist male + pristane animals developed autoantibodies to smRNP, Smith proteins, U1-A, and U1-68, but the levels

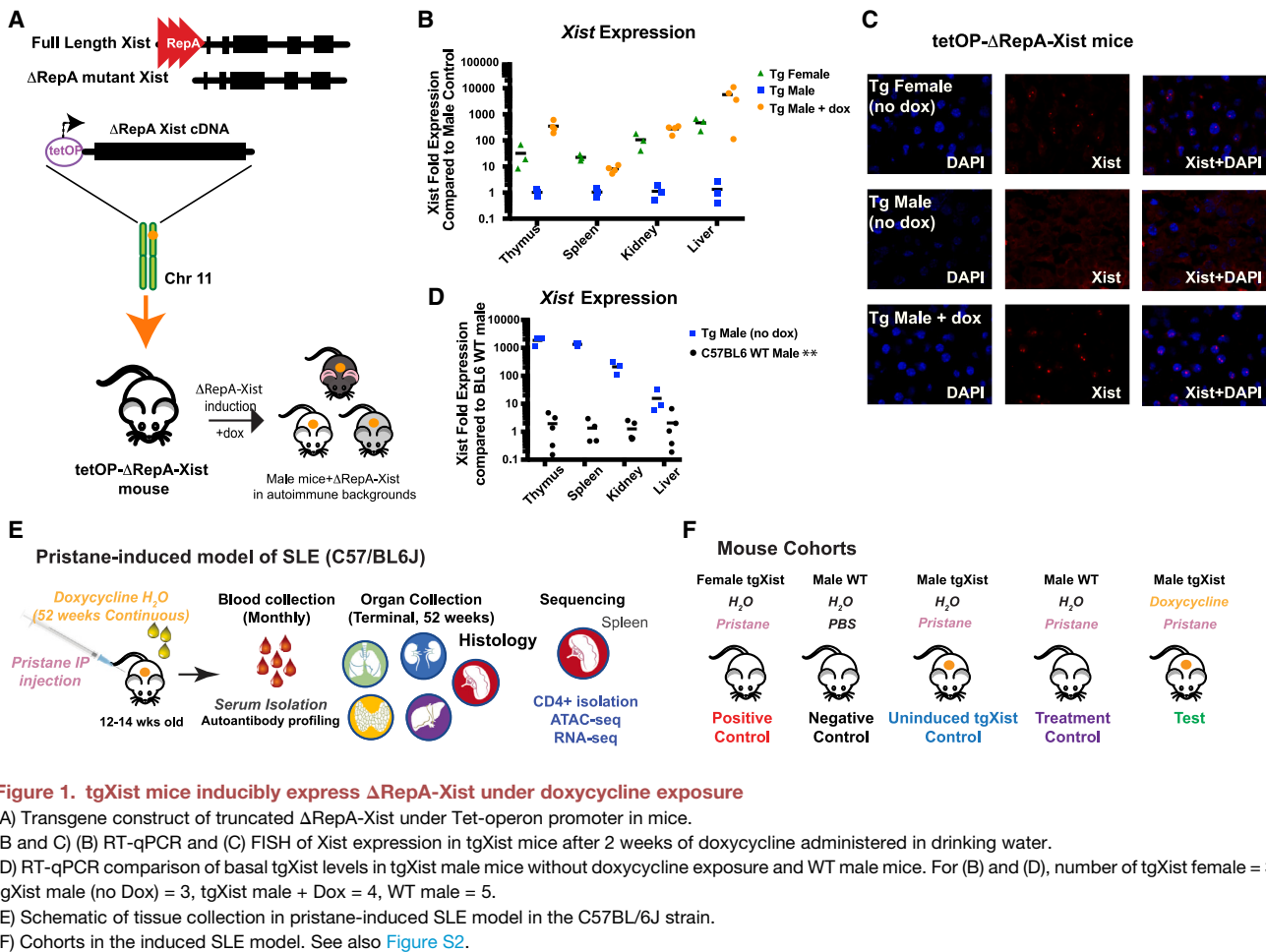


**Figure 1. tgXist mice inducibly express  $\Delta$ RepA-Xist under doxycycline exposure**

(A) Transgene construct of truncated  $\Delta$ RepA-Xist under Tet-operon promoter in mice. (B and C) (B) RT-qPCR and (C) FISH of Xist expression in tgXist mice after 2 weeks of doxycycline administered in drinking water. (D) RT-qPCR comparison of basal tgXist levels in tgXist male mice without doxycycline exposure and WT male mice. For (B) and (D), number of tgXist female = 3, tgXist male (no Dox) = 3, tgXist male + Dox = 4, WT male = 5. (E) Schematic of tissue collection in pristane-induced SLE model in the C57BL/6J strain. (F) Cohorts in the induced SLE model. See also Figure S2.

were heterogeneous. These results indicate that in the non-permissive C57/BL6 background, these animals have a low propensity to develop autoantibody or organ disease after an inflammatory challenge, and tgXist did not bypass this genetic barrier.

### Transgenic Xist drives males to female-like changes in T cell profiles

While pristane treatment in C57BL/6J mice did not manifest disease, splenic CD4<sup>+</sup> T cells (an important cell type for balancing and driving autoimmunity<sup>25–27</sup>) from tgXist-expressing male mice showed molecular changes more similar to those in females than to control (tgXist-non-induced/WT) males at several levels. Potential changes in the transcriptional regulation and gene expression of CD4<sup>+</sup> splenic T cells were assessed using assay of transposase accessible chromatin by sequencing (ATAC-seq) and RNA sequencing (RNA-seq) of multiple animals per cohort at 52 weeks post-treatment (Figures 2A and S3C–S3E). Global comparison of ATAC-seq differential peaks showed several differences between non-tgXist-/Xist-expressing animals, compared with tgXist-expressing males and WT Xist-expressing females, but very few differential peaks between females compared with males expressing tgXist (Figure 2B). Principal-component analysis (PCA) comparison of female mice, male mice, and male tgXist-expressing mice (male +

Dox) showed a separation of mice most highly correlated with sex (Figure 2C). Three of six tgXist-expressing male mice showed female-like skewing (circled in Figure 2C), in keeping with the expected female penetrance percentage.

ATAC-seq revealed distinct clusters of accessibility corresponding to tgXist-/Xist-expressing and non-expressing mice (Figure 2D). tgXist-induced and pristane-injected males displayed similar chromatin accessibility to pristane-injected female positive control mice, with higher accessibility in cluster 2, and were distinct from male negative control groups (tgXist non-induced and WT) that displayed higher accessibility in cluster 1 (Figure 2D). Interestingly, the top Reactome categories in cluster 2, associated with tgXist-expressing males and Xist-expressing females, displayed high Toll-like receptor (TLR) pathway signatures (Figure 2E) not present in cluster 1 (Figure S3D). *Tlr9*, encoding a pathogen sensor in the innate immune pathway that is highly active in SLE, is significantly more accessible in females and tgXist-induced males (Figure S3E). RNA-seq profiles of gene expression displayed a similar trend and clustering grouped by tgXist/Xist expression with some variability within cohorts (Figures 2F and S3C), suggesting that ATAC-seq provides a more consistent profile of cells in transition. Comparison of dysregulated genes from ATAC- and RNA-seq revealed an overlap of 364 genes (Figure 2G). CIBERSORT<sup>28</sup>

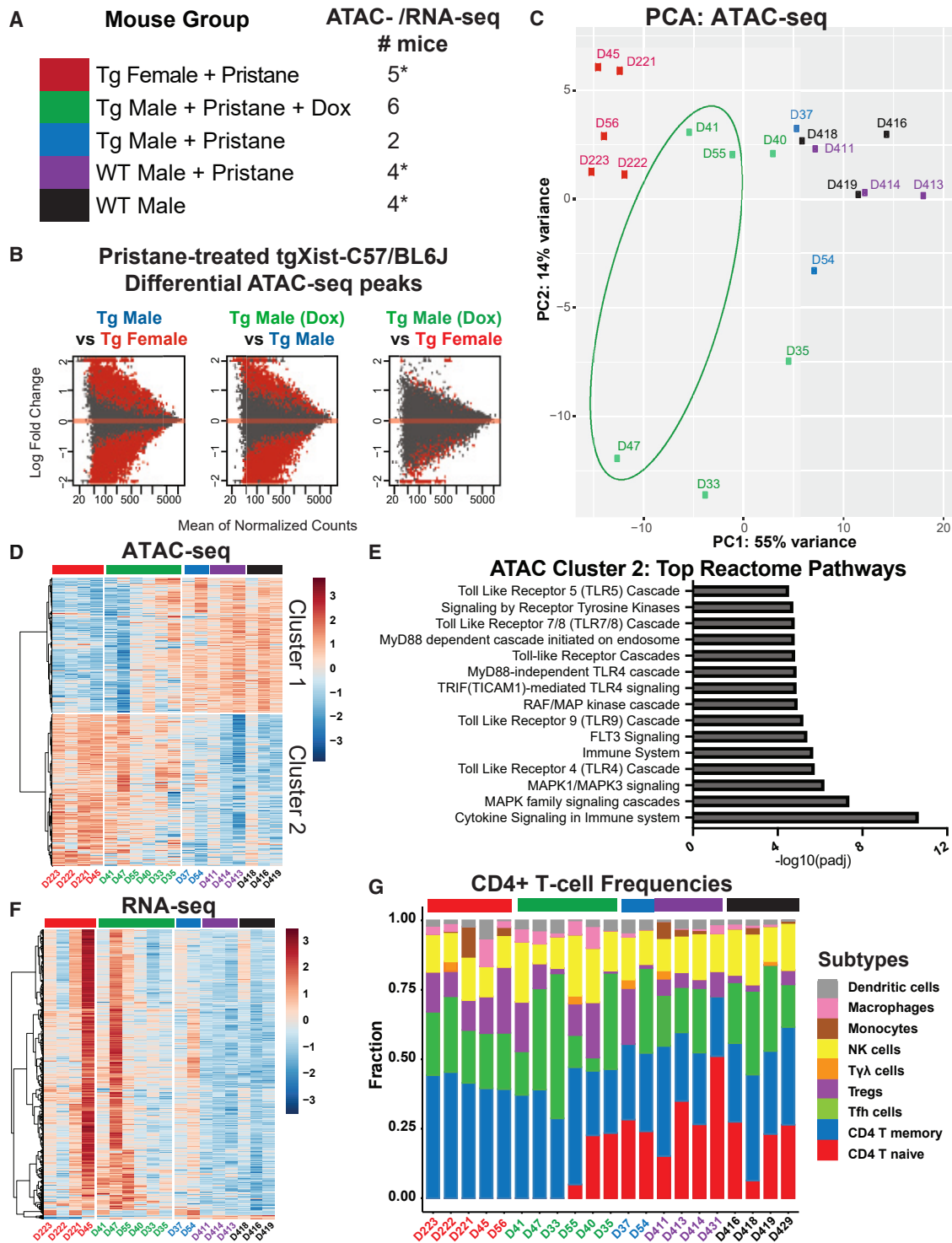


**Figure 2. Bulk ATAC-seq and RNA-seq of splenic CD4+ T cells from C57BL/6J mice reveal closer correlation between tgXist- and Xist-expressing mice in the pristane-induced SLE model**

(A) Table of treatment cohorts: colors correspond to each treatment cohort, and numbers indicate the number of ATAC-seq and RNA-seq samples. \*Due to library quality, one of the ATAC-seq libraries was excluded.

(B) MA plots comparing differential regions of genomic accessibility in transgenic cohorts.

(C) Principal-component analysis (PCA) plots of ATAC-seq libraries from all mice in the study.

(legend continued on next page)

deconvolution of gene expression signatures also identified a clear segregation of *Xist*-expressing and non-expressing mice. In particular, *tgXist*- or *Xist*-expressing males and WT females, respectively, contained more CD4 memory T cells, whereas control males expressed greater proportions of naive T cells (Figure 2G).

### **Xist expression in males promotes multi-organ autoimmune pathology**

We next tested the effect of *tgXist* expression in the autoimmune-prone SJL/J mouse background, a widely used strain in multiple autoimmune disease models.<sup>22,29,30</sup> Pristane-induced SLE in SJL/J mice exhibits many characteristics of human SLE, such as autoantibody development, TLR7 upregulation, and multi-organ involvement, and demonstrates a strong female bias.<sup>10,22</sup> SJL/J female mice display earlier mortality, more severe nephritis, and higher levels of autoantibodies, and they are 3.4× more likely to die than male mice.<sup>22</sup> This disease model is also more reflective of most human patients than spontaneous SLE models that are restricted to specific genetic mutations.<sup>31–34</sup>

We administered a one-time 0.5 mL intraperitoneal injection of pristane to 8- to 10-week-old mice to induce SLE in *tgXist* and WT mice, and continuous ingestion of Dox was supplied in drinking water to activate *tgXist* in selected mice (Figure 3A). The experimental cohorts include the WT female pristane-treated positive control, negative controls of mock-injected *tgXist* and WT males, the WT male treatment control, and the test group of *tgXist*-expressing pristane-treated males (Figure 3B; Table S2). Since previous literature determined that WT SJL/J females display mortality as early as 16 weeks post-pristane injection,<sup>22</sup> we selected the terminal time point of 16 weeks post-injection to avoid premature loss of mice.

As SLE is a systemic disease, we used H&E staining to assess the pathology of multiple affected organs at the terminal collection time on a disease scale of 0–5 for each individual organ (Figures 3C and 3D). In all pristane-treated cohorts, pristane injection caused lipogranulomas in adipose tissues, lymph node hyperplasia and medullary plasmacytosis, as well as varying degrees of extramedullary hematopoiesis and lymphoid expansion in the spleen. However, pristane injection coupled with *tgXist* expression in males or *Xist* in WT females resulted in greater incidence and severity of glomerulonephritis (kidney), hepatic lipogranulomas (liver), and pulmonary hemorrhage and lymphohistiocytic alveolitis (lung), which are reflective of disease damage in the kidney, liver, and lungs observed in severe SLE patients<sup>35</sup> (Figure 3C). Manifestation of mild signs of early SLE in some pristane-injected male controls was not unexpected because WT SJL/J males are expected to develop milder disease and display later mortality at 24 weeks post-injection.<sup>22</sup>

To assess whether *Xist* expression induced female-level autoimmune disease, we summed the disease scores across 6 organs in individual animals and chose the total pathology score of 10 as the cutoff for severe disease, which clearly distinguished

WT female mice treated with pristane (positive control) vs. WT male mice treated with pristane (treatment control). Every female mouse had a score of 10 or above; none of the male WT mice treated with pristane met this cutoff ( $p = 2.01E-6$ , Fisher's exact test). In *tgXist* males treated with pristane, the total pathology increased in a bimodal fashion, compared with WT males: 5 of 8 mice achieved female-level pathology (score > 10), while 3 animals had much less disease severity ( $p = 0.009$ , false discovery rate [FDR] < 0.05) (Figure 3E). Concordantly, the greatest statistical difference was observed in the comparison between the female positive controls and the pristane-treated WT males ( $p = 2.01E-6$ ), and the significance lessened in the comparison between females and *tgXist* males treated with pristane ( $p = 0.042$ , FDR < 0.05) (Figure 3E). Thus, a majority of *tgXist* male mice experienced female-level severe pathology in the pristane-induced SLE model.

Sera collected at treatment start (day 0, baseline) and terminally (16 weeks post-treatment) were assessed for reactivity to known SLE and scleroderma (SSc) antigens using the Luminex bead-based antigen array.<sup>36</sup> We found 4 known autoantibodies (RIBO P0, RIBO P2, CENPA, and CENPB) that are elevated in female WT mice vs. male WT mice treated with pristane. The mean level is increased for all four autoantibodies in *tgXist* male mice + pristane vs. WT male mice + pristane but with different degrees of variance. Anti-CENPB is significantly elevated in *tgXist* male mice treated with pristane vs. WT male mice treated with pristane ( $p = 0.02$ , FDR < 0.05), and the former is no longer significantly different from WT female mice. The other three antibodies showed an intermediate picture. They are elevated in only a subset of *tgXist* male + pristane animals; they are no longer significantly different from WT female animals with disease, but they are not statistically significant compared with WT male control (Figure 3F). The heterogeneity of known autoantibodies may track with disease severity; all five of the animals in the *tgXist* male + pristane cohort with severe disease had the highest level of anti-RIBO P2 (Figures 3F and S4).

### **Single-cell ATAC analysis reveals distinct cell-type clustering and consistent reformatting of the chromatin landscape in pristane-treated SJL/J animals**

To gain insight to the genes and cellular processes underpinning the heightened autoimmunity in *tgXist*- and *Xist*-expressing mice, we created single-cell ATAC+ gene expression libraries of CD45+ (pan-hematopoietic)-sorted splenic cells from pristane-injected mice in the SJL/J strain. A key advantage of the single-cell multi-omics approach is the ability to interrogate all the hematopoietic lineages within the spleen in a single assay. While our bulk ATAC-seq and RNA-seq in the C57BL/6J strain was restricted to CD4+ T cells, the single-cell libraries encompass the whole CD45+ splenic population.

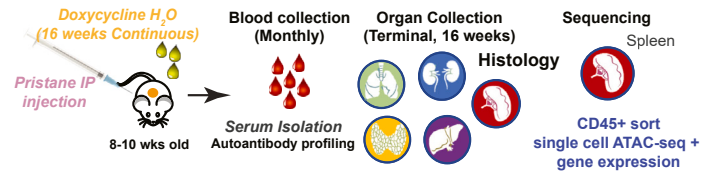
Using the total lowest observed pathology score in female mice (10) as the cutoff (Figures 3B and 3D), we divided the pristane-induced *tgXist*-expressing males into high (total pathology

(D and F) Heatmap of (D) ATAC-seq Z scores and (F) RNA-seq differential gene expression. Differential peak and gene lists generated from comparisons of the Tg female+ pristane, WT male (mock treatment), and Tg male + pristane (no Dox) groups to WT male + pristane cohort.

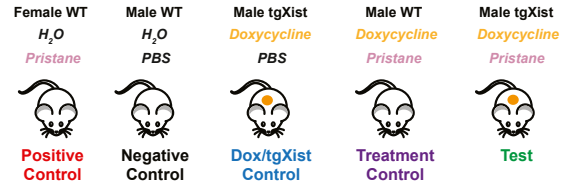
(E) Top 15 differential Reactomes associated with cluster 2 genomic regions.

(G) CIBERSORT prediction of T cell subset composition from CD4+ T cells RNA-seq gene expression libraries. See also Figure S3 and Table S2.

**A** Pristane-induced model of SLE



**B** Mouse Cohorts

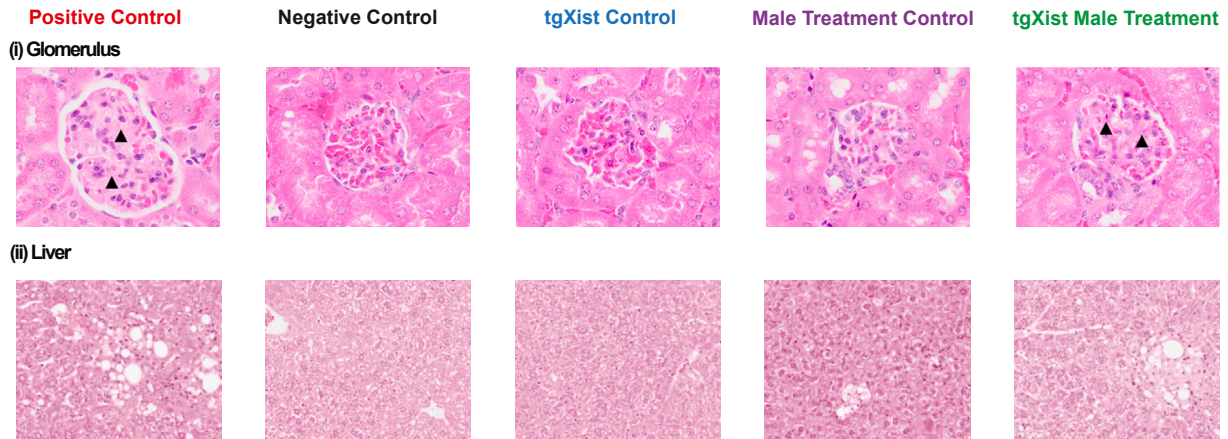


**C** Scoring of SLE pathology in organs

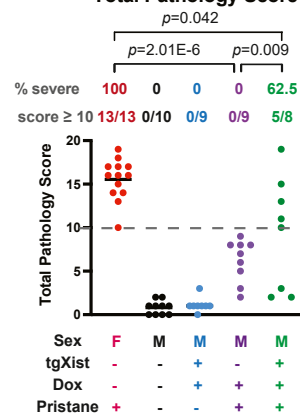
Mouse Group	Sex	Genotype	Treatment	#	Kidney	Liver	Spleen	Adipose	Lung	Lymph Nodes	Total
Positive Control	F	WT	Pristane+H <sub>2</sub> O	13	2.46 ± 1.13	3.15 ± 0.69	4.23 ± 1.24	1 ± 0	3.77 ± 1.09	0.92 ± 0.28	15.54 ± 2.37
Negative Control	M	WT	PBS+H <sub>2</sub> O	10	0	0	0.80 ± 0.79	0	0	0	0.80 ± 0.79
tgXist (Dox) Control	M	TgXist	PBS+Dox	9	0	0	0.89 ± 0.60	0	0	0.11 ± 0.33	1.00 ± 0.87
Male Treatment Control	M	WT	Pristane+Dox	9	0.44 ± 0.73	0.67 ± 0.87	2.56 ± 1.01	0.78 ± 0.44	1.11 ± 1.05	0.67 ± 0.50	6.22 ± 2.44
tgXist Male Treatment	M	TgXist	Pristane+Dox	8	1.38 ± 1.19	1.75 ± 1.67	3.00 ± 1.51	0.63 ± 0.52	2.13 ± 1.96	0.50 ± 0.33	9.38 ± 6.44

Damage scale:  
0 = Within Normal Limits  
3 = Moderate  
5 = Severe

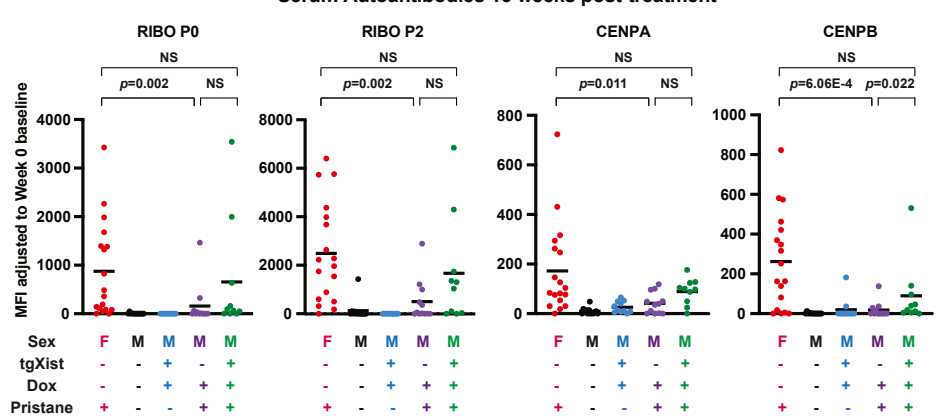
**D**



**E** Total Pathology Score



**F** Serum Autoantibodies 16 weeks post-treatment



(legend on next page)

score  $\geq 10$ ) and low ( $<10$ ) disease groups. Sequencing libraries were made from representative mice selected from the tgXist male high disease (tgM high,  $n = 4$ ), tgXist male low disease (tgM low,  $n = 4$ ), and two pristane-injected control groups: WT females (WT F,  $n = 4$ ) and WT males (WT M,  $n = 3$ ). Due to high mitochondrial/ribosomal RNA content, 2 of the WT females were excluded from the gene expression analysis. To maintain consistency, we included only cells with both ATAC and gene expression reads.

The single-cell ATAC uniform manifold approximation and projection (UMAP) formed 19 clusters (Figure S5A) and were assigned cell-type identities using imputation of key marker genes (Figures 4A and S5C). The four pristane-treated mouse groups were generally evenly distributed across all clusters, although tgM high mice contained a higher fraction of cells within the CD4 T cell cluster (Figure 4B). TgM high cells also formed a visually separate CD4\_Tcell and Bcell\_1 group on the UMAP (Figures 4A and 4C), but comparison of distinguishing markers did not show prominent differences from the adjacent CD4\_Tcell and Bcell\_1 populations. As expected, the tgXist male mice and female mice all showed peaks in the first *Xist* exon region (the *Xist* transcription start site is absent in the *Xist* transgene), which are lacking in the WT control males (Figure 4D).

Interestingly, WT F and tgM high cells appear to overlap in the main Bcell\_2 cluster (Figures 4A and 4C), which co-localizes *Cd19* with the atypical B cell marker *Zeb2* (Figure S5C). However, pairwise comparisons between the mouse groups did not identify significant differences in the chromatin landscape within the main lymphocyte clusters, even when comparing the most distinct positive disease control (WT F) to the males with the lowest disease scores (WT M and tgM low) (Figure S5D). Aside from a higher CD4T cell fraction in the tgM high mice and atypical B cell activation markers, there were few noticeable distinguishing features in the single-cell ATAC comparisons between the pristane-treated mouse groups, suggestive that all of the pristane-treated mice in the autoimmune-prone SJL/J model may have already undergone epigenetic remodeling preceding physiological disease onset at the time of investigation (16 weeks post-injection).

### Single-cell gene expression analysis reveals elevation of atypical B cells and suppression of T cell modulators in diseased tgXist animals

We next interrogated the pristane-treated SJL/J groups by single-cell gene expression, which may reflect cell states with greater immediacy. The single-cell gene expression UMAP formed 12 distinct clusters and were segregated clearly into B

cell, T cell, natural killer (NK) cell, and myeloid and erythroid lineages, based on key transcription factors and markers (Figures 5A and S6A). The cellular-type identities assigned to cells in the gene expression clusters closely matched the ATAC cell-type identities (Figure S5B), further validating the consistency of the assigned cellular identities in both the ATAC and gene expression datasets.

Within the B cell cluster, the tgXist male high disease group is overlaid with the female WT mice, distinct from the WT male and the relatively unaffected tgXist male low disease animals (Figures 5B, S6B, and S7A–S7D). Since B cells produce the majority of autoantibodies and proinflammatory cytokines that characterize autoimmune pathogenesis,<sup>37,38</sup> the high correlation of B cells, specifically of the tgXist-diseased males with those from positive disease control females, provides another layer of support for the hypothesis that Xist complexes mediate an environment of higher autoimmunity. The tgXist low disease and WT males grouped closely together, and most of the differences between the tgXist high disease and WT female mice lay in the sex chromosomes or ribosomal protein genes. Inspection of the differentially expressed genes, comparing the disease-affected tgXist male and female mice with the WT males (Figure S6C), revealed that the majority of both downregulated and upregulated genes were shared between the first two groups (Figure 5C). Particularly significant genes included the upregulation of the atypical B cell marker *Zeb2* (tgM high vs. WT M,  $p = 3.08E-69$ , WT F vs. WT M,  $p = 1.17E-35$ ) and *CD22* (tgM high vs. WT M,  $p = 7.63E-46$ , WT F vs. WT M  $p = 2.59E-36$ ), a receptor associated with pathogenic B cells<sup>39</sup> critical for B cell proliferation and B cell receptor signaling (Figure S6D). Concurrently, *Siglec-g*, encoding a receptor associated with promoting B cell self-tolerance, deficiency of which is associated with increased B-1 cells and multiple autoimmune diseases,<sup>40–42</sup> was significantly downregulated (tgM high vs. WT M,  $p = 1.73E-101$ , WT F vs. WT M,  $p = 1.01E-43$ ) (Figure S6D). Also downregulated were complement receptor 2 (*Cr2*, tgM high vs. WT M,  $p = 1.30E-153$ , WT F vs. WT M  $p = 3.70E-44$ ) and the paralog to its alternatively spliced form, *Cr1l* (tgM high vs. WT M,  $p = 4.41E-33$ , WT F vs. WT M,  $p = 1.35E-33$ ), both of which are important for suppressing autoimmunity.<sup>43,44</sup>

Within the B cell clusters, WT F and tgM high uniquely overlapped in a region of Bcell\_3 not populated by either WT M or tgM low disease groups (Figures S7A–S7D). Cluster Bcell\_3 contained the highest correlation of gene expression signatures of atypical B cell markers<sup>45</sup> (Figure S7E, highlighted in orange), including upregulation of *Cd19*, *Ms4a1* (gene encoding Cd20), *Zeb2*, and *Fcrl5*, a defining marker of atypical memory B cells

### Figure 3. Increased pathophysiology and autoantibody levels in tgXist- and Xist-expressing mice in the SJL/J strain in the pristane-induced SLE model

(A) Schematic of pristane-induced SLE and strategy for histopathology, serum, and sequencing analysis in the SJL/J strain.

(B) Treatment cohorts in the SJL/J strain.

(C) Table of the mean severity of damage across multiple tissue sites and mice.

(D) Representative H&E images of (i) glomeruli (kidney) and (ii) liver sections from each treatment cohort. Arrows demarcate mesangial thickening.

(E) Graph of total sum of pathophysiology damage scores. Significance calculated using Fisher's exact test and  $FDR < 0.05$ .

(F) Median fluorescence intensity (MFI) of serum reactivity to autoantigens, using a bead-based lupus antigen array after 16 weeks of treatment. Significance calculated using the unpaired Wilcoxon rank-sum test and values displayed at  $FDR < 0.05$ . Number of mouse serum samples, listed from left to right: wild-type female + pristane = 18, wild-type male negative control = 13, tgXist male + Dox (tgXist control) = 11, wild-type male treatment = 12, tgXist male treatment = 10. p values are indicated; NS indicates not significant or not meeting  $FDR < 0.05$ . See also Figure S4 and Tables S2 and S7.

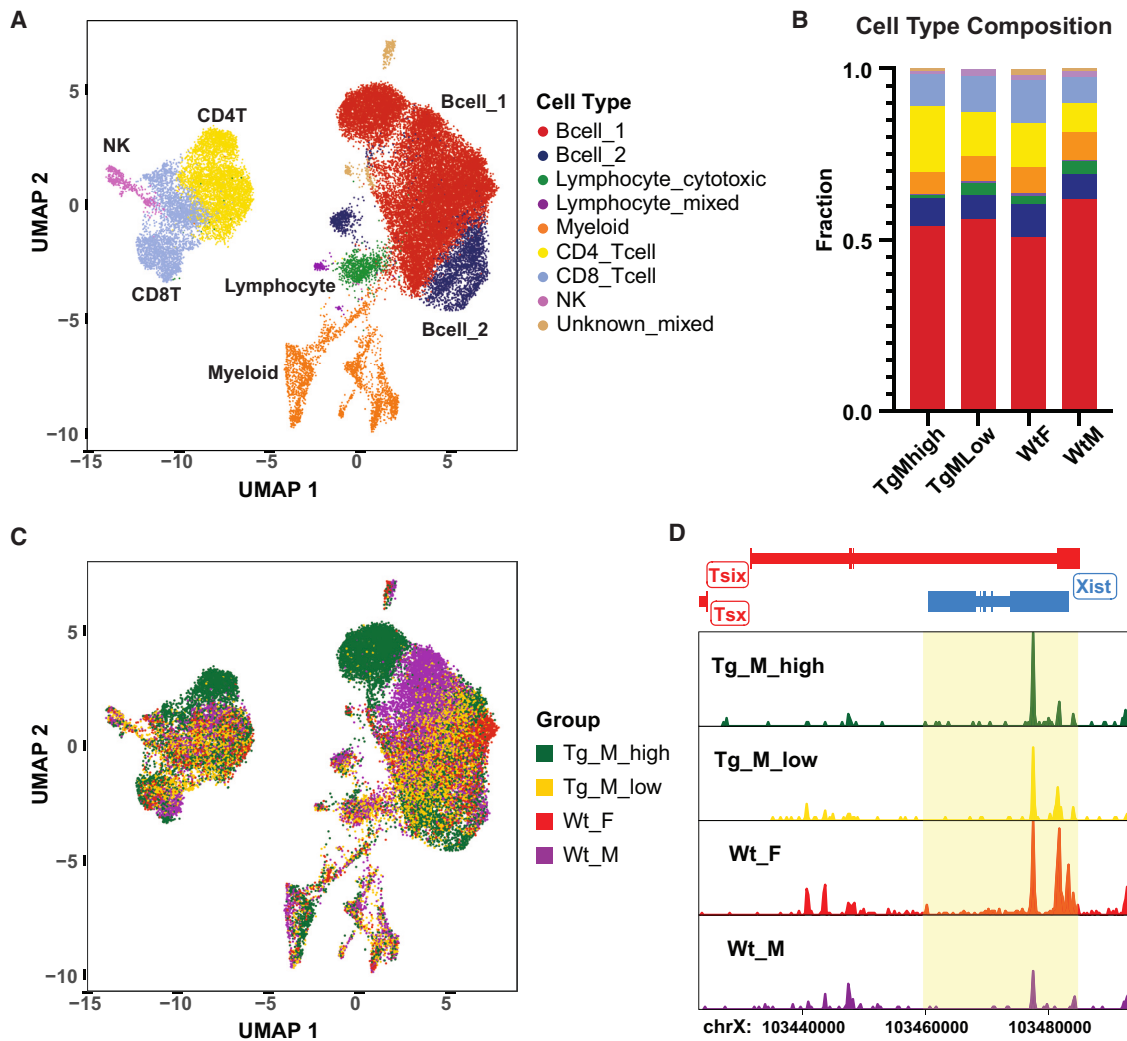


**Figure 4. Single-cell ATAC comparisons of splenic CD45<sup>+</sup> hematopoietic cells from pristane-treated mice in the SJL/J strain**

(A and B) (A) UMAP of cell-type cluster identities and (B) corresponding cell-type composition within each pristane-treated mouse group.

(C and D) (C) UMAP clustering and (D) *Xist* peak tracks from pristane-treated mouse groups (features FDR  $\leq$  0.1 and  $\log_2$  FC  $\geq$  0.5). Pristane-treated mouse groups shown: tgXist male, disease high (n = 4); tgXist male, disease low (n = 4); wild-type male (n = 3); and wild-type female (n = 2). See also Figure S5.

in both mice and humans,<sup>46</sup> as well as downregulation of *Cr2* (*Cd21*), *Cd27*, and *Cxcr5*.<sup>47,48</sup> Furthermore, Bcell\_3 cluster cells from the gene expression data matched solely to the independently clustered multiome ATAC UMAP Bcell\_2 cell clusters (Figure S5B), the ATAC clusters imputed to have atypical B cell characteristics (Figure S5C, *Zeb2* imputation). Closer examination of the gene expression Bcell\_3 cluster showed significant elevation of *Zeb2* (tgM high vs. WT M,  $p = 6.12E-74$ , WT F vs. WT M,  $p = 8.53E-9$ ) and downregulation of *Cr2* (tgM high vs. WT M,  $p = 1.75E-89$ , WT F vs. WT M,  $p = 3.03E-14$ ) and *Cxcr5* (tgM high vs. WT M,  $p = 5.65E-23$ , WT F vs. WT M,  $p = 2.61E-18$ ) in high disease, compared with relatively unaffected mouse groups (representative plots, Figure 5D). CD21<sup>−</sup>CD27<sup>−</sup> double negative are typical distinguishers of atypical B cells while loss of CXCR5 in CD21<sup>−</sup> effector B cells is a hallmark of atypical B cells in SLE pathogenesis in patients.<sup>47,48</sup>

While the UMAP within the T cell clusters was less distinctly demarcated than the B cell cluster (Figures 5B and S6E), the overall pattern was clear in the shared downregulated programs (Figure 5E). Multiple key T cell regulation and self-tolerance genes were downregulated in the tgXist male high disease and female cohorts, compared with the WT males. Among the significantly downregulated genes were the glucocorticoid receptor *Nr3c1* (tgM high vs. WT M,  $p = 1.37E-33$ , WT F vs. WT M,  $p = 1.33E-63$ ) involved in Treg modulation of inflammation,<sup>49</sup> *Cd37* (tgM high vs. WT M,  $p = 4.60E-12$ , WT F vs. WT M,  $p = 1.81E-10$ ) that regulates proliferation<sup>50</sup> and complement-mediated apoptosis of autoreactive T cells,<sup>50</sup> the CD4 T cell immune regulator *Cd52*<sup>51</sup> (tgM high vs. WT M,  $p = 7.24E-13$ , WT F vs. WT M,  $p = 2.22E-72$ ), and invariant chain *Cd74* involved in training antigen immunity in T cells<sup>52</sup> (tgM high vs. WT M,  $p = 8.15E-37$ , WT F vs. WT M  $p = 2.27E-96$ ) (representative plots, Figure 5F).

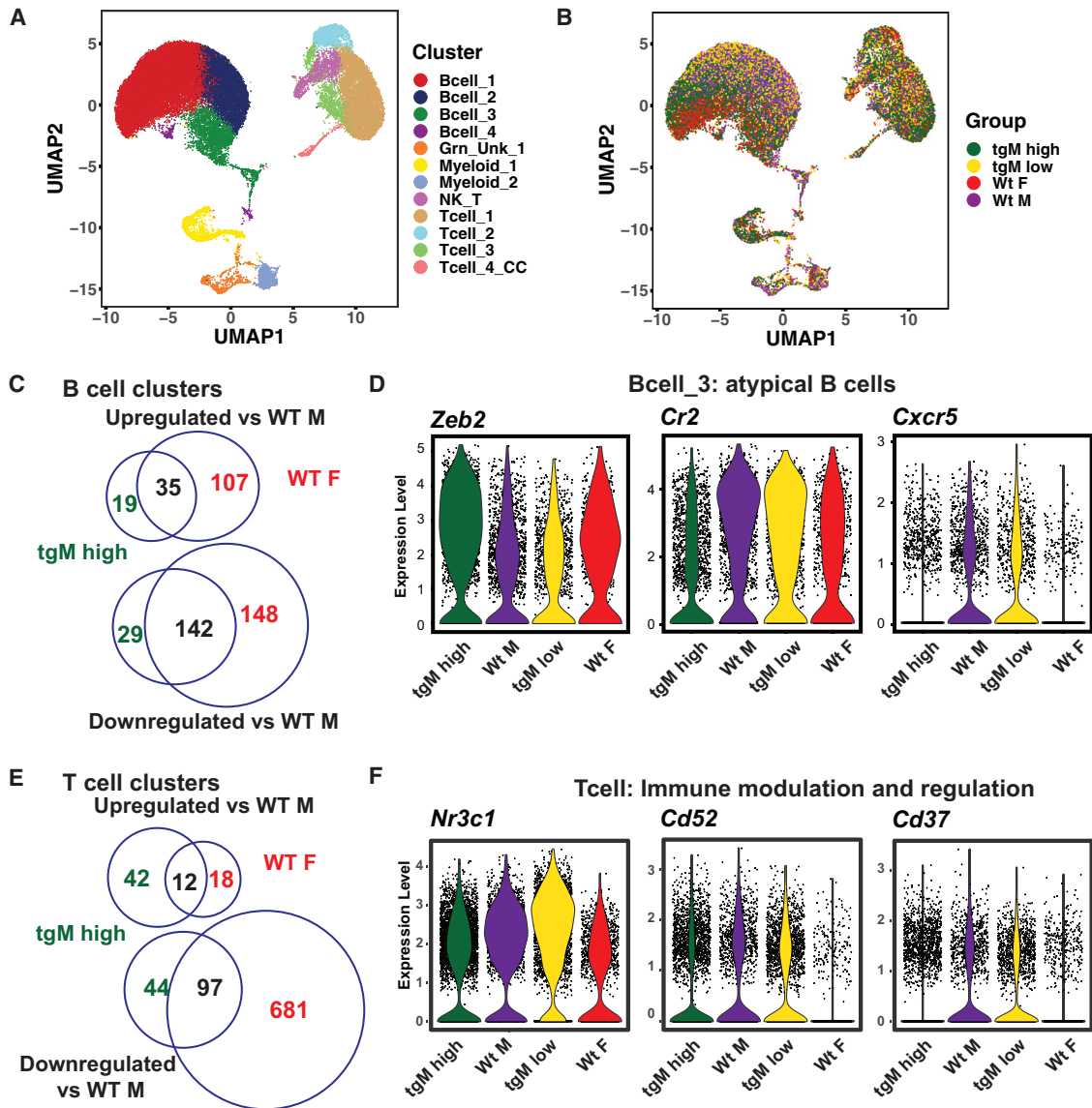


**Figure 5. Single-cell gene expression comparisons of splenic CD45+ hematopoietic cells from pristane-treated mice in the SJL/J strain** (A and B) (A) Cell-type cluster identities and (B) pristane-treated mouse groups displayed on the single-cell gene expression clustering UMAP. (C) Metrics of differentially expressed B cell cluster genes of tgXist male high disease and wild-type female compared with wild-type male. (D and E) (D) Representative gene expression plots of atypical B cell genes from the Bcell\_3 cluster, and (E) metrics of differentially expressed T cell cluster genes of tgXist male high disease and wild-type female compared with wild-type male. (F) T cell cluster highlighting significant differentially expressed genes. Pristane-treated mouse groups shown: tgXist male, disease high (n = 4); tgXist male, disease low (n = 4); wild-type male (n = 3); and wild-type female (n = 2). Significance was calculated using the Wilcoxon rank-sum test. See also Figures S6 and S7.

Our multiome sequencing identified clusters suggestive of atypical B cells overlapping closely in both ATAC and gene expression. At the single-cell gene expression level, the severity of disease in tgXist-/Xist-expressing animals may be driven by increased atypical B cell activity and decreased immune modulatory programs in both B and T cells. Combined with the heightened pathophysiology scores and increased autoantigen levels, the gene expression data corroborate a role for *Xist* RNPs in the development of increased and/or more severe autoimmunity in the pristane-induced SLE model.

#### Autoimmune patients and mice display multiple autoantibodies to the XIST RNP

The imperfect association of known autoantibodies with tgXist-enhanced disease motivated us to consider whether novel autoantibodies to Xist RNP itself exist in human patients. To test whether the XIST RNP is immunogenic in humans, we obtained de-identified sera from patients with dermatomyositis (DM), SSc, and SLE to test for reactivity to XIST complex proteins.<sup>12,14</sup> We used protein fragments produced by the Human Protein Atlas for 130 XIST-associated proteins of interest (selection described

in STAR Methods) and 52 for control proteins used as clinical markers for DM, SSc, and SLE. Three of the clinical protein antigens overlapped with the XIST ChIRP-MS lists (SSB, SNRPD2, and SRP14). When possible, multiple fragments spanning different regions of each protein were used (Figure 6A).

As a general population control, we obtained serum from anonymous donations to the Stanford Blood Center. However, since the mean and median age of these donors were 58 and 61 years at the time of donation, these donors may express some autoreactivity due to advanced age. Nevertheless, autoimmune patients were significantly more reactive to 55 proteins, 16 of which were disease markers, 1 of which overlapped with XIST RNP (SSB), and the remaining 39 antigens from the XIST RNP list (Figure 6B; Table S5). Distinct reactive antigens for each autoimmune disease arose when grouped by disease (Figure 6C), and 9 antigens were shared among all 3 diseases (Figure 6D; Table S5). Of these, TRIM33, or TIF1- $\gamma$ , is a clinical marker for autoimmune disease (DM).<sup>53</sup> The other 8 were XIST RNP components, several of which have recently discovered roles in autoimmunity. HMGB1 was recently identified as an autoantigen in SLE/Sjögren that may be another SS-protein in the SS-A/SS-B family,<sup>54,55</sup> HNRNPK is an autoantigen in a subset of Raynaud's disease<sup>56,57</sup> and aplastic anemia, SAFB is a novel autoantigen in connective tissues detected in interstitial lung disease, and XPO5 is in the SSB/La processing pathway.<sup>58</sup>

In sum, the 3 disease groups were significantly reactive to 79 unique proteins in the array, compared with the general population control. Of these 79 proteins, 27 were disease controls, and 53 were associated with the XIST RNP (SSB is also a disease control marker). Furthermore, 37 of the 53 XIST-associated proteins were part of the group of 118 high-confidence published XIST RNP complex proteins.<sup>14</sup> Of these 37 high-confidence XIST complex proteins, 28 have not been described in the current published literature as autoantigens associated with autoimmune disease and are potentially novel biomarkers (Table S5). These results show that multiple proteins from the XIST RNPs are novel autoantigens in patients with DM, SSc, and SLE.

Finally, we turned to our mouse model to probe the drivers of autoantibodies to Xist RNP. Using our Xist RNP array, we analyzed sera from the tgXist mice of the SJL/J background to examine the effect of tgXist and pristane-induced lupus. We compared sera of each animal longitudinally at 0, 4, 12, and 16 weeks after treatment across 5 mouse cohorts, allowing us to infer a causal relationship between perturbation and autoantibodies to Xist RNP. We compared the autoantibodies in tgXist mice with autoantibodies to the same proteins in human patients with SLE, which grounds the mouse results with human disease relevance (Figure 7A). First, we observed that female WT mice treated with pristane induced dozens of autoantibodies to Xist RNP by 12 weeks, which persist through 16 weeks. These Xist RNP autoantibodies significantly overlap autoantibodies to Xist RNP in human patients with SLE ( $p = 0.001$ , Figure 7B). Second, tgXist expression in males treated with pristane induced many of the same antibodies against Xist RNP, which are at higher levels than in WT male mice treated with pristane at both 12 and 16 weeks ( $p = 6 \times 10^{-11}$  and  $p = 1 \times 10^{-29}$ , respectively, revised Figures 7B–7D). Third, high levels of Xist RNP antibodies are only observed in pristane-

treated mice, indicating a key role for tissue damage and inflammation. Moreover, WT female mice had higher Xist RNP antibodies than tgXist male mice (both treated with pristane) at 12 weeks after treatment ( $p < 7 \times 10^{-37}$ ); tgXist male mice only reached female level of Xist RNP antibodies at 16 weeks (revised Figures 7C and 7D). These results show that tgXist expression in males can promote autoantibodies to Xist RNP in the context of tissue damage, but this occurs with slower kinetics than in WT females.

## DISCUSSION

### Xist lncRNA as a polymeric antigen scaffold in female-biased autoimmunity

Our study nominates Xist RNP complexes as antigenic triggers underlying the greater prevalence of autoimmune diseases in females. Although it is a well-documented fact that females are more prone to autoimmune diseases than males, previous studies primarily examined differences in gene dosage and hormonal background. While prior studies of Xist address altered X inactivation and the subsequent impact of XCI escape of X-linked genes,<sup>14,59,60</sup> this study investigated the immunogenicity of Xist RNP complex itself. We have shown that expression of Xist RNPs in male mice is sufficient to increase disease severity and change the expression and epigenomic profiles of both the B cell and T cell effectors of SLE pathogenesis.

Physicians and scientists have long noted that many autoantibodies target large nucleic acid-protein complexes, such as chromatin or RNP, in human autoimmune diseases. This feature was exploited by molecular biologists using patient sera to identify components of the centromere (recognized by autoantibodies in calcinosis, Raynaud's phenomenon, esophageal dysmotility, sclerodactyly, telangiectasia [CREST] syndrome) or spliceosome (SLE and DM). Immunologists have explained this phenomenon with the idea that large nucleic acid-protein complexes are polymeric, and if exposed in the extracellular space, they can cluster and activate immunoreceptors. We propose that the XIST RNP is one such dominant antigenic array that is unique to females. Every cell in a woman's body has XIST, which is a long polymer (19 kb) and coats the entire inactive X chromosome in the condensed Barr body (an even larger polymer). When a female cell dies due to tissue injury, XIST RNPs will invariably be exposed to the immune system. Our data further suggest a model where XIST contributes to several steps in the progression to autoimmune disease (Figure 7C). In a genetically autoimmune-resistant background, a low level of XIST, even in the presence of tissue injury, leads to only changes in T cell subsets and chromatin states but not to frank organ pathology. These epigenetic changes in accessibility are then subsequently reflected in the gene expression programs upregulating autoreactivity and downregulating immune modulation. Finally, in the context of a permissive genetic background and repeated tissue injury, the presence of XIST RNP exacerbates full-blown end organ pathology and activation of multiple immune cell types. Longitudinal studies of sera reactivity and autoimmune disease in humans are consistent with this model.<sup>61</sup>

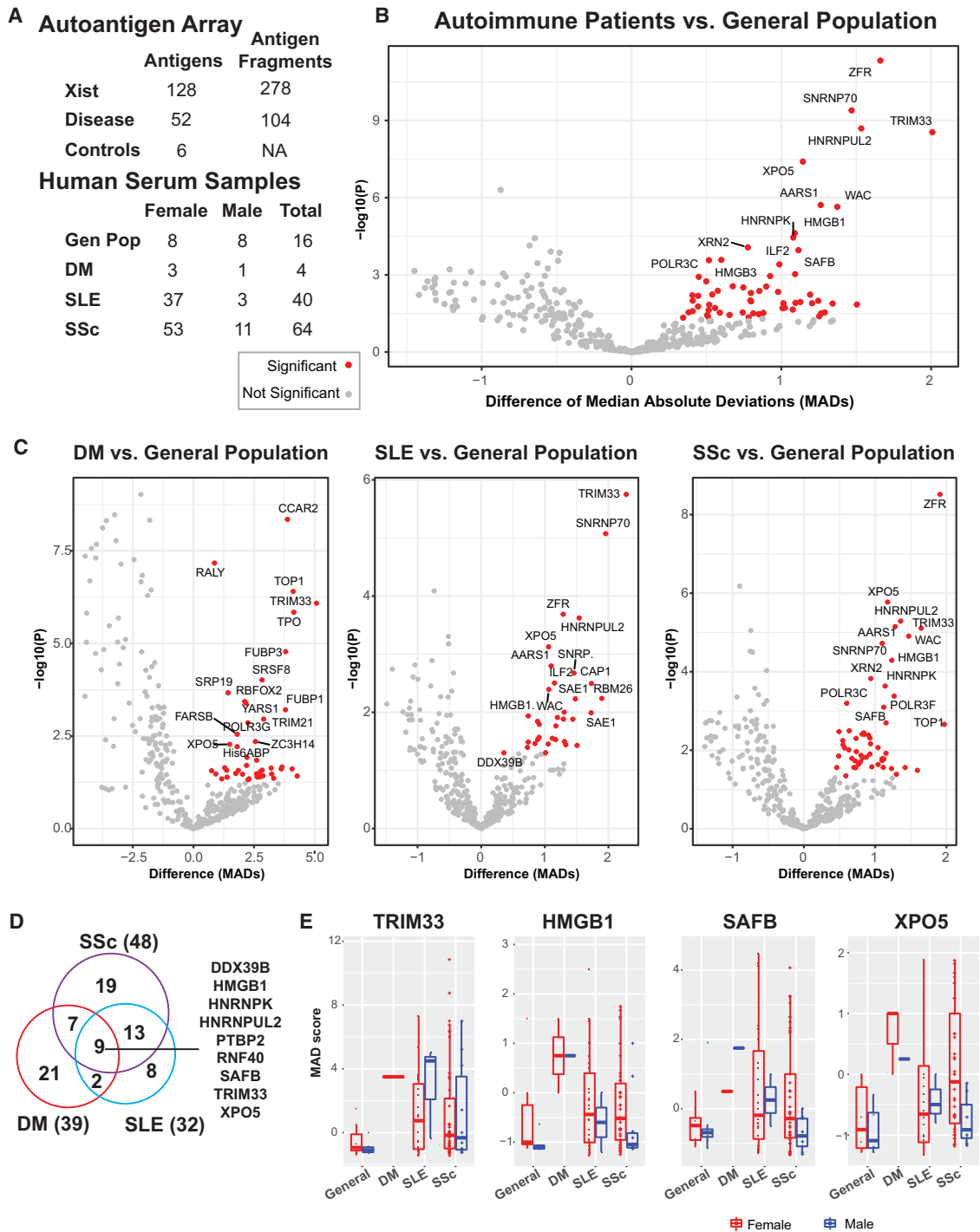


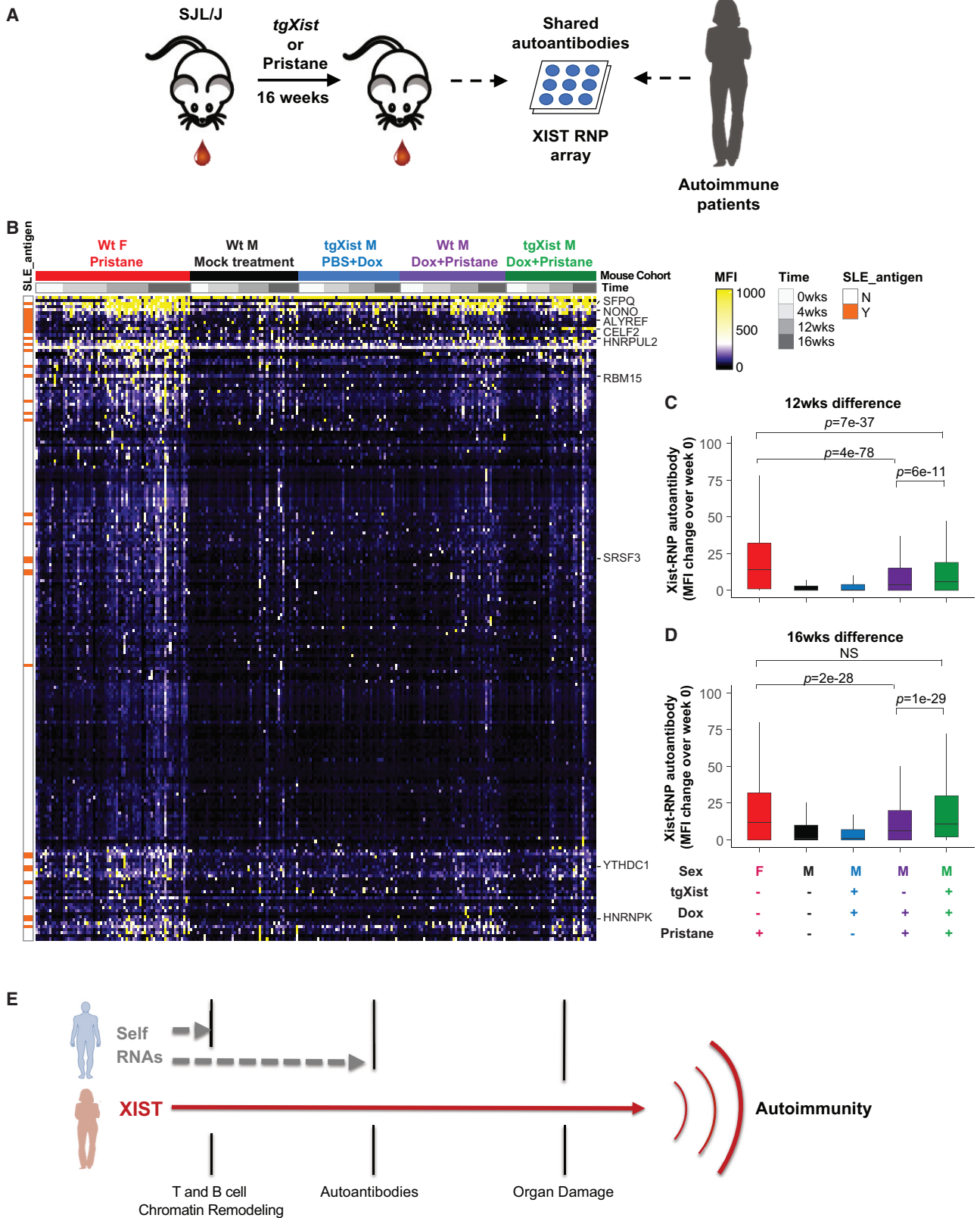
**Figure 6. Autoimmune disease patients experience increased serum reactivity toward antigens of the XIST RNP**

(A) Table of the XIST complex-associated antigen array design showing the number of total unique proteins and corresponding protein fragments counts drawn from XIST ChIRP-MS, clinical disease panel, and control protein lists; and sample numbers of autoimmune patient and general population serum.

(B and C) (B) Volcano plot of serum reactivity of all autoimmune patients, and (C) sera grouped by DM, SSc, and SLE patients, compared with general population baseline of serum from blood donors. Significant differentially reactive antigens, defined as  $p_{adj} < 0.05$  and median absolute deviation (MAD) difference  $> 0$ , labeled in red. Significance calculated using the Student's t test.

(D) Metrics of unique antigens from the array with significant elevated serum activity in autoimmune patients, compared with the general population.

(E) Serum reactivity (MAD) plots of representative antigens significantly reactive in all three autoimmune patient cohorts grouped by disease type and colored by sex (red, female; blue, male). See also Figure S1 and Tables S1, S4, and S5.



(legend on next page)

### Opportunities for disease diagnosis and therapy

There are more than 100 known autoimmune diseases that in aggregate afflict ~50 million Americans and comprise one of the top ten leading causes of death for women under the age of 65.<sup>62</sup> Worryingly, cases are increasing yearly on a global scale, and recent serologic studies revealed a steep rise of increasing ANA reactivity.<sup>63,64</sup> Understanding the risk factors and drivers of autoimmunity has become even more critical in the race to develop effective therapies and sensitive diagnostics specific to each autoimmune disease. However, the high heterogeneity within autoimmune diseases and overlapping traits across diseases have limited our ability to tailor effective therapies and sensitive diagnostics specific to each autoimmune disease.<sup>65</sup> Our discovery of seropositivity toward multiple XIST-associating proteins in autoimmune patients introduces a novel antigen set with clinical potential for enhancing disease detection and monitoring, as autoantibodies are often detected prior to or early in disease onset.<sup>61,66</sup> In addition, studies in SSc have also demonstrated the effectiveness of autoantigen analysis in patient stratification and of identifying pathogenic pathways.<sup>67,68</sup> Profiling the XIST RNP in primary cells, both healthy and diseased, may be useful in advancing our understanding of the aberrant autoreactivity toward proteins within the complex and in identifying more potential autoantigens.

Currently, there are few targeted therapies for autoimmune diseases available. The most common therapies involve B cell depletion but are not always effective. There remains a need for more specific pathogenic leukocyte targets. We identified atypical B cells as a population of immune cells that accumulates as a consequence of Xist RNP expression. Atypical B cells (also known as age-associated B cells) are a unique population of B cells that expands with increased TLR7 signaling<sup>69,70</sup> and in female-biased autoimmunity.<sup>71</sup> Notably, atypical B cells accumulate in aged female mice but not in age-matched male mice,<sup>69</sup> and atypical B cells are enriched in human or mouse B cells that escape XCI and re-express *TLR7*.<sup>14,72</sup> Thus, atypical B cells appear as the immunological nexus of two potential consequences of mammalian dosage compensation—autoreactivity to Xist RNP and escape from XCI—and suggest that these consequences may synergize to promote female-biased immunity. Future studies should address whether and how atypical B cells or other cell types evoked by Xist RNP contribute to autoimmunity.

### Limitations of the study

This study employs a truncated Xist missing the RepA to model Xist RNP action in male mice. The detection of autoantibodies to Xist RNP in female patients and WT female mice indicates that tgXist models important aspects of full-length Xist in females. Although we have confirmed that immune cell subsets, autoantibodies, and disease penetrance of autoimmunity of tgXist males are at an intermediate level between WT male and WT female, arguing against a neomorphic effect of Xist-ΔRepA, it is formally possible that Xist-ΔRepA differentially impacts other features of autoimmunity. Fragmentation of cell-free Xist RNP is the inevitable consequence as the complex is released from dying cells and eventually cleared, and this interpretation is fully compatible with our model for female-biased immunity. Our transgenic model expressed Xist ubiquitously in male animals, and the role of individual tissues or cell types most responsible for the observed phenotypes and the required time window of Xist RNP exposure should be dissected in future studies. Additionally, a known limitation of Tet-regulated expression cassettes is that they can be leaky or silenced over time *in vivo*.<sup>73–76</sup> Thus, there is likely variability or decline of tgXist expression in our transgenic model during the experiment; and the level of Xist required to confer female-level autoimmune risk is unclear. Similarly, this work has not addressed whether fluctuations in Xist level in female individuals may impact autoimmunity. Finally, this study employed a modest number of animals and patient samples, and several results showed large variation between test subjects. Future studies with larger numbers and a detailed focus on exactly which XIST-related antigens contribute to female-biased immunity will be valuable.

### STAR★METHODS

Detailed methods are provided in the online version of this paper and include the following:

- KEY RESOURCES TABLE
- RESOURCE AVAILABILITY
  - Lead contact
  - Materials availability
  - Data and code availability
- EXPERIMENTAL MODELS AND STUDY PARTICIPANT DETAILS
  - Mouse Strains
  - Clinical Cohorts

### Figure 7. Model of XIST RNP in autoimmune progression

(A) Schematic using the Xist antigen array to identify autoantibodies shared in SLE patients and tgXist-/Xist-expressing SJL/J mice with/without pristane-induced SLE.

(B) Antibody reactivity (MFI normalized to bare bead baseline) against Xist RNP members is shown for the five indicated mouse cohorts across time points. Xist RNP members that are also autoantigens in human SLE patients are indicated on left bar (SLE\_antigens). Each row is a Xist RNP member; each column is a mouse serum sample.

(C and D) (C) Quantification of Xist RNP autoantibody reactivity at 12 weeks after treatment and (D) at 16 weeks after treatment. Significant p values are indicated (Wilcoxon rank-sum test, all with FDR < 0.05); non-significant differences are indicated with “NS.” Heatmap and boxplot visualization plots capped at 1,000 MFI to account for outliers. Number of mouse serum samples: wild-type female + pristane = 18, wild-type male mock treatment = 13, tgXist male PBS + Dox = 11, wild-type male Dox + pristane = 12, tgXist male Dox + pristane = 10.

(E) Autoreactivity to Xist RNPs first causes changes in the chromatin landscape impacting genomic accessibility and changes in lymphocyte gene expression programs prefiguring the development of autoantibodies, and it cascades to prolonged autoreactive activity, damaging organs in the final stages of autoimmunity. See also Figure S1 and Table S5.

- **METHOD DETAILS**
  - Induction and evaluation of pristane-induced SLE in mice
  - Sequencing Library Preparation
  - Computational Analysis of Sequencing Libraries
  - SLE autoantigen Panel Array
  - XIST Autoantigen Array
- **QUANTIFICATION AND STATISTICAL ANALYSES**

### SUPPLEMENTAL INFORMATION

Supplemental information can be found online at <https://doi.org/10.1016/j.cell.2023.12.037>.

### ACKNOWLEDGMENTS

We thank members of the Chang and Utz labs for discussion and Adrienne Woods and Gwendolyn Leatherman for assistance with serum compilation from Johns Hopkins. We thank Greg S. Nelson for assistance with mouse blood collection, the Stanford Veterinary Service Center and the Stanford Breeding Colony Management Services for assistance with animal husbandry and welfare, the Stanford Comparative Medicine Services for histology preparation, the Stanford Transgenic, Knockout and Tumor Model Research Center for tissue sample preparation, the Stanford Functional Genomics Facility for bulk sequencing assistance, and the Stanford Shared FACS Facility for assistance in cell sorting. This work was supported by Scleroderma Research Foundation (H.Y.C.), NIAMS T32 AR007422 and NIAMS K99/R00 (D.R.D.), and NIAMS T32 AR050942 (B.T.A.). The Hopkins Lupus Cohort is supported by a grant from the National Institute of Arthritis and Musculoskeletal Diseases under award R01-AR069572. H.Y.C. is an Investigator and J.A.B. is a Hanna Gray Fellow of the Howard Hughes Medical Institute.

### AUTHOR CONTRIBUTIONS

Conceptualization, D.R.D., P.J.U., and H.Y.C.; methodology and investigation, D.R.D., K.M.C., R.L., D.C.C., K.K., C.H., R.S., S.C., A.F., D.W.G., A.A.S., M.P., L.S.C., D.F.F., and A.W.; data analysis, D.R.D., Y.Z., J.A.B., S.S., Y.Z., K.M.C., B.Y., B.T.A., C.H., R.S., A.F., and E.K.L.; writing, D.R.D., K.M.C., L.S.C., D.F.F., P.J.U., and H.Y.C.; funding acquisition, H.Y.C.; resources, H.Y.C.; supervision, H.Y.C.

### DECLARATION OF INTERESTS

H.Y.C. is a co-founder of Accent Therapeutics, Boundless Bio, Cartography Biosciences, and Orbital Therapeutics and an advisor to 10x Genomics, Arsenal Biosciences, Chroma Medicine, and Spring Discovery. A.A.S. receives research grant funding from the following companies to support clinical trials in SSc: Arena Pharmaceuticals, Eicos Sciences, Kadmon Corporation, and Medpace.

Received: February 28, 2023  
Revised: October 3, 2023  
Accepted: December 31, 2023  
Published: February 1, 2024

### REFERENCES

1. Fairweather, D., and Rose, N.R. (2004). Women and autoimmune diseases. *Emerg. Infect. Dis.* *10*, 2005–2011.
2. Libert, C., Dejager, L., and Pinheiro, I. (2010). The X chromosome in immune functions: when a chromosome makes the difference. *Nat. Rev. Immunol.* *10*, 594–604.
3. Fairweather, D., Frisnacho-Kiss, S., and Rose, N.R. (2008). Sex differences in autoimmune disease from a pathological perspective. *Am. J. Pathol.* *173*, 600–609.
4. Moulton, V.R. (2018). Sex Hormones in Acquired Immunity and Autoimmune Disease. *Front. Immunol.* *9*, 2279.
5. Syrett, C.M., Sierra, I., Beethem, Z.T., Dubin, A.H., and Anguera, M.C. (2020). Loss of epigenetic modifications on the inactive X chromosome and sex-biased gene expression profiles in B cells from NZB/W F1 mice with lupus-like disease. *J. Autoimmun.* *107*, 102357.
6. Syrett, C.M., Sindhava, V., Sierra, I., Dubin, A.H., Atchison, M., and Anguera, M.C. (2018). Diversity of Epigenetic Features of the Inactive X-Chromosome in NK Cells, Dendritic Cells, and Macrophages. *Front. Immunol.* *9*, 3087.
7. Subramanian, S., Tus, K., Li, Q.Z., Wang, A., Tian, X.H., Zhou, J., Liang, C., Bartov, G., McDaniel, L.D., Zhou, X.J., et al. (2006). A Tlr7 translocation accelerates systemic autoimmunity in murine lupus. *Proc. Natl. Acad. Sci. USA* *103*, 9970–9975.
8. Christensen, S.R., Shupe, J., Nickerson, K., Kashgarian, M., Flavell, R.A., and Shlomchik, M.J. (2006). Toll-like receptor 7 and TLR9 dictate autoantibody specificity and have opposing inflammatory and regulatory roles in a murine model of lupus. *Immunity* *25*, 417–428.
9. Scofield, R.H., Bruner, G.R., Namjou, B., Kimberly, R.P., Ramsey-Goldman, R., Petri, M., Reveille, J.D., Alarcón, G.S., Vilá, L.M., Reid, J., et al. (2008). Klinefelter's syndrome (47,XXY) in male systemic lupus erythematosus patients: support for the notion of a gene-dose effect from the X chromosome. *Arthritis Rheum.* *58*, 2511–2517.
10. Smith-Bouvier, D.L., Divekar, A.A., Sasidhar, M., Du, S., Tiwari-Woodruff, S.K., King, J.K., Arnold, A.P., Singh, R.R., and Voskuhl, R.R. (2008). A role for sex chromosome complement in the female bias in autoimmune disease. *J. Exp. Med.* *205*, 1099–1108.
11. Awate, S., Babiuk, L.A., and Mutwiri, G. (2013). Mechanisms of action of adjuvants. *Front. Immunol.* *4*, 114.
12. Chu, C., Zhang, Q.C., da Rocha, S.T., Flynn, R.A., Bharadwaj, M., Calabrese, J.M., Magnuson, T., Heard, E., and Chang, H.Y. (2015). Systematic discovery of Xist RNA binding proteins. *Cell* *161*, 404–416.
13. McHugh, C.A., Chen, C.K., Chow, A., Surka, C.F., Tran, C., McDonel, P., Pandya-Jones, A., Blanco, M., Burghard, C., Moradian, A., et al. (2015). The Xist lncRNA interacts directly with SHARP to silence transcription through HDAC3. *Nature* *521*, 232–236.
14. Yu, B., Qi, Y., Li, R., Shi, Q., Satpathy, A.T., and Chang, H.Y. (2021). B cell-specific XIST complex enforces X-inactivation and restrains atypical B cells. *Cell* *184*, 1790–1803.e17.
15. Lau, C.M., Broughton, C., Tabor, A.S., Akira, S., Flavell, R.A., Mamula, M.J., Christensen, S.R., Shlomchik, M.J., Vigiñanti, G.A., Rifkin, I.R., et al. (2005). RNA-associated autoantigens activate B cells by combined B cell antigen receptor/Toll-like receptor 7 engagement. *J. Exp. Med.* *202*, 1171–1177.
16. Busconi, L., Lau, C.M., Tabor, A.S., Uccellini, M.B., Ruhe, Z., Akira, S., Vigiñanti, G.A., Rifkin, I.R., and Marshak-Rothstein, A. (2006). DNA and RNA autoantigens as autoadjuvants. *J. Endotoxin Res.* *12*, 379–384.
17. Means, T.K., Latz, E., Hayashi, F., Murali, M.R., Golenbock, D.T., and Luster, A.D. (2005). Human lupus autoantibody-DNA complexes activate DCs through cooperation of CD32 and TLR9. *J. Clin. Invest.* *115*, 407–417.
18. Wutz, A., Rasmussen, T.P., and Jaenisch, R. (2002). Chromosomal silencing and localization are mediated by different domains of Xist RNA. *Nat. Genet.* *30*, 167–174.
19. Giorgetti, L., Lajoie, B.R., Carter, A.C., Attia, M., Zhan, Y., Xu, J., Chen, C.J., Kaplan, N., Chang, H.Y., Heard, E., et al. (2016). Structural organization of the inactive X chromosome in the mouse. *Nature* *535*, 575–579.
20. Graham, K.L., Thibault, D.L., Steinman, J.B., Okeke, L., Kao, P.N., and Utz, P.J. (2005). Granzyme B is dispensable for immunologic tolerance to self in a murine model of systemic lupus erythematosus. *Arthritis Rheum.* *52*, 1684–1693.
21. Izui, S., Higaki, M., Morrow, D., and Merino, R. (1988). The Y chromosome from autoimmune BXSB/MpJ mice induces a lupus-like syndrome

- in (NZW x C57BL/6)F1 male mice, but not in C57BL/6 male mice. *Eur. J. Immunol.* **18**, 911–915.
22. Smith, D.L., Dong, X., Du, S., Oh, M., Singh, R.R., and Voskuhl, R.R. (2007). A female preponderance for chemically induced lupus in SJL/J mice. *Clin. Immunol.* **122**, 101–107.
  23. Satoh, M., Richards, H.B., Shaheen, V.M., Yoshida, H., Shaw, M., Naim, J.O., Wooley, P.H., and Reeves, W.H. (2000). Widespread susceptibility among inbred mouse strains to the induction of lupus autoantibodies by pristane. *Clin. Exp. Immunol.* **121**, 399–405.
  24. Reeves, W.H., Lee, P.Y., Weinstein, J.S., Satoh, M., and Lu, L. (2009). Induction of autoimmunity by pristane and other naturally occurring hydrocarbons. *Trends Immunol.* **30**, 455–464.
  25. Luckheeram, R.V., Zhou, R., Verma, A.D., and Xia, B. (2012). CD4<sup>+</sup>T cells: differentiation and functions. *Clin. Dev. Immunol.* **2012**, 925135.
  26. Barron, L., and Wynn, T.A. (2011). Fibrosis is regulated by Th2 and Th17 responses and by dynamic interactions between fibroblasts and macrophages. *Am. J. Physiol. Gastrointest. Liver Physiol.* **300**, G723–G728.
  27. Palmer, M.T., and Weaver, C.T. (2010). Autoimmunity: increasing suspects in the CD4<sup>+</sup> T cell lineup. *Nat. Immunol.* **11**, 36–40.
  28. Newman, A.M., Steen, C.B., Liu, C.L., Gentles, A.J., Chaudhuri, A.A., Scherer, F., Khodadoust, M.S., Esfahani, M.S., Luca, B.A., Steiner, D., et al. (2019). Determining cell type abundance and expression from bulk tissues with digital cytometry. *Nat. Biotechnol.* **37**, 773–782.
  29. Storer, J.B. (1966). Longevity and gross pathology at death in 22 inbred mouse strains. *J. Gerontol.* **21**, 404–409.
  30. Constantinescu, C.S., Farooqi, N., O'Brien, K., and Gran, B. (2011). Experimental autoimmune encephalomyelitis (EAE) as a model for multiple sclerosis (MS). *Br. J. Pharmacol.* **164**, 1079–1106.
  31. Celhar, T., and Fairhurst, A.M. (2017). Modelling clinical systemic lupus erythematosus: similarities, differences and success stories. *Rheumatology (Oxford)* **56** (Suppl 1), i88–i99.
  32. Morel, L. (2004). Mouse models of human autoimmune diseases: essential tools that require the proper controls. *PLoS Biol.* **2**, E241.
  33. Bender, A.T., Wu, Y., Cao, Q., Ding, Y., Oestreicher, J., Genest, M., Akare, S., Ishizaka, S.T., and Mackey, M.F. (2014). Assessment of the translational value of mouse lupus models using clinically relevant biomarkers. *Transl. Res.* **163**, 515–532.
  34. Perry, D., Sang, A., Yin, Y., Zheng, Y.Y., and Morel, L. (2011). Murine Models of Systemic Lupus Erythematosus. *J. Biomed. Biotechnol.* **2011**, 271694.
  35. Cojocaru, M., Cojocaru, I.M., Silosi, I., and Vrabie, C.D. (2011). Manifestations of systemic lupus erythematosus. *Maedica (Bucur)* **6**, 330–336.
  36. Degn, S.E., van der Poel, C.E., Firl, D.J., Ayoglu, B., Al Qureshah, F.A., Bajic, G., Mesin, L., Reynaud, C.A., Weill, J.C., Utz, P.J., et al. (2017). Clonal Evolution of Autoreactive Germinal Centers. *Cell* **170**, 913–926.e19.
  37. Musette, P., and Bouaziz, J.D. (2018). B Cell Modulation Strategies in Autoimmune Diseases: New Concepts. *Front. Immunol.* **9**, 622.
  38. Lee, D.S.W., Rojas, O.L., and Gommerman, J.L. (2021). B cell depletion therapies in autoimmune disease: advances and mechanistic insights. *Nat. Rev. Drug Discov.* **20**, 179–199.
  39. Clark, E.A., and Giltiay, N.V. (2018). CD22: A Regulator of Innate and Adaptive B Cell Responses and Autoimmunity. *Front. Immunol.* **9**, 2235.
  40. Müller, J., Lunz, B., Schwab, I., Acs, A., Nimmerjahn, F., Daniel, C., and Nitschke, L. (2015). Siglec-G Deficiency Leads to Autoimmunity in Aging C57BL/6 Mice. *J. Immunol.* **195**, 51–60.
  41. Brzezicka, K.A., and Paulson, J.C. (2023). Impact of Siglecs on autoimmune diseases. *Mol. Aspects Med.* **90**, 101140.
  42. Poe, J.C., and Tedder, T.F. (2012). CD22 and Siglec-G in B cell function and tolerance. *Trends Immunol.* **33**, 413–420.
  43. Holers, V.M., and Boackle, S.A. (2004). Complement receptor 2 and autoimmunity. *Curr. Dir. Autoimmun.* **7**, 33–48.
  44. Song, W.C. (2006). Complement regulatory proteins and autoimmunity. *Autoimmunity* **39**, 403–410.
  45. Sutton, H.J., Aye, R., Idris, A.H., Vistein, R., Nduati, E., Kai, O., Mwacharo, J., Li, X., Gao, X., Andrews, T.D., et al. (2021). Atypical B cells are part of an alternative lineage of B cells that participates in responses to vaccination and infection in humans. *Cell Rep.* **34**, 108684.
  46. Li, H., Dement-Brown, J., Liao, P.J., Mazo, I., Mills, F., Kraus, Z., Fitzsimmons, S., and Tolnay, M. (2020). Fc receptor-like 4 and 5 define human atypical memory B cells. *Int. Immunol.* **32**, 755–770.
  47. Jenks, S.A., Cashman, K.S., Zumaquero, E., Marigorta, U.M., Patel, A.V., Wang, X., Tomar, D., Woodruff, M.C., Simon, Z., Bugrovsky, R., et al. (2018). Distinct Effector B Cells Induced by Unregulated Toll-like Receptor 7 Contribute to Pathogenic Responses in Systemic Lupus Erythematosus. *Immunity* **49**, 725–739.e6.
  48. Gao, X., and Cockburn, I.A. (2022). The development and function of CD11c<sup>+</sup> atypical B cells – insights from single cell analysis. *Front. Immunol.* **13**, 979060.
  49. Engler, J.B., Kursawe, N., Solano, M.E., Patas, K., Wehrmann, S., Heckmann, N., Lühder, F., Reichardt, H.M., Arck, P.C., Gold, S.M., et al. (2017). Glucocorticoid receptor in T cells mediates protection from autoimmunity in pregnancy. *Proc. Natl. Acad. Sci. USA* **114**, E181–E190.
  50. Oostindie, S.C., van der Horst, H.J., Lindorfer, M.A., Cook, E.M., Tupitza, J.C., Zent, C.S., Burack, R., VanDerMeid, K.R., Strumane, K., Chamuleau, M.E.D., et al. (2019). CD20 and CD37 antibodies synergize to activate complement by Fc-mediated clustering. *Haematologica* **104**, 1841–1852.
  51. Toh, B.H., Kyaw, T., Tipping, P., and Bobik, A. (2013). Immune regulation by CD52-expressing CD4 T cells. *Cell. Mol. Immunol.* **10**, 379–382.
  52. Mensali, N., Grenov, A., Pati, N.B., Dillard, P., Myhre, M.R., Gaudernack, G., Kvalheim, G., Inderberg, E.M., Bakke, O., and Wälchli, S. (2019). Antigen-delivery through invariant chain (CD74) boosts CD8 and CD4 T cell immunity. *Oncoimmunology* **8**, 1558663.
  53. Satoh, M., Tanaka, S., Ceribelli, A., Calise, S.J., and Chan, E.K. (2017). A Comprehensive Overview on Myositis-Specific Antibodies: New and Old Biomarkers in Idiopathic Inflammatory Myopathy. *Clin. Rev. Allergy Immunol.* **52**, 1–19.
  54. Chen, M., Zhou, Y., Xue, M., Zhu, R., Jing, L., Lin, L., He, C., and Qin, Y. (2022). Anti-HMGB1 antibody is a potential characteristic autoantibody for Sjögren's syndrome. *Sci. Rep.* **12**, 6020.
  55. Takeuchi, A., Matsushita, T., Kaji, K., Okamoto, Y., Yasui, M., Hirata, M., Oishi, N., Higashi, A., Seishima, M., Asano, T., et al. (2017). Autoantibody to scaffold attachment factor B (SAFB): A novel connective tissue disease-related autoantibody associated with interstitial lung disease. *J. Autoimmun.* **76**, 101–107.
  56. Yang, L., Fujimoto, M., Murota, H., Serada, S., Fujimoto, M., Honda, H., Yamada, K., Suzuki, K., Nishikawa, A., Hosono, Y., et al. (2015). Proteomic identification of heterogeneous nuclear ribonucleoprotein K as a novel cold-associated autoantigen in patients with secondary Raynaud's phenomenon. *Rheumatol. Oxf. Engl.* **54**, 349–358.
  57. Qi, Z., Takamatsu, H., Espinoza, J.L., Lu, X., Sugimori, N., Yamazaki, H., Okawa, K., and Nakao, S. (2010). Autoantibodies specific to hnRNP K: a new diagnostic marker for immune pathophysiology in aplastic anemia. *Ann. Hematol.* **89**, 1255–1263.
  58. Hasler, D., Lehmann, G., Murakawa, Y., Klironomos, F., Jakob, L., Grässer, F.A., Rajewsky, N., Landthaler, M., and Meister, G. (2016). The Lupus Autoantigen La Prevents Mis-channeling of tRNA Fragments into the Human MicroRNA Pathway. *Mol. Cell* **63**, 110–124.
  59. Mousavi, M.J., Mahmoudi, M., and Ghotloo, S. (2020). Escape from X chromosome inactivation and female bias of autoimmune diseases. *Mol. Med.* **26**, 127.
  60. Syrett, C.M., Paneru, B., Sandoval-Heglund, D., Wang, J., Banerjee, S., Sindhava, V., Behrens, E.M., Atchison, M., and Anguera, M.C. (2019).

Altered X-chromosome inactivation in T cells may promote sex-biased autoimmune diseases. *JCI Insight* 4, e126751.

61. Arbuckle, M.R., McClain, M.T., Rubertone, M.V., Scofield, R.H., Dennis, G.J., James, J.A., and Harley, J.B. (2003). Development of autoantibodies before the clinical onset of systemic lupus erythematosus. *N. Engl. J. Med.* 349, 1526–1533.
62. Walsh, S.J., and Rau, L.M. (2000). Autoimmune diseases: a leading cause of death among young and middle-aged women in the United States. *Am. J. Public Health* 90, 1463–1466.
63. Lerner, A., Patricia, W., and Matthias, T. (2015). The World Incidence and Prevalence of Autoimmune Diseases is Increasing. *Int. J. Celiac Dis.* 3, 151–155.
64. Dinse, G.E., Parks, C.G., Weinberg, C.R., Co, C.A., Wilkerson, J., Zeldin, D.C., Chan, E.K.L., and Miller, F.W. (2020). Increasing Prevalence of Antinuclear Antibodies in the United States. *Arthritis Rheumatol.* 72, 1026–1035.
65. Jury, E.C., D’Cruz, D., and Morrow, W.J.W. (2001). Autoantibodies and overlap syndromes in autoimmune rheumatic disease. *J. Clin. Pathol.* 54, 340–347.
66. Rosen, A., and Casciola-Rosen, L. (2016). Autoantigens as Partners in Initiation and Propagation of Autoimmune Rheumatic Diseases. *Annu. Rev. Immunol.* 34, 395–420.
67. Dou, D.R., Zhao, Y., Abe, B., Li, R., Zaba, L.C., Aren, K., Carns, M., Chung, L.S., Hinchcliff, M., and Chang, H.Y. (2021). Distinct T cell chromatin landscapes in scleroderma subtypes. Preprint at bioRxiv.
68. Xu, G.J., Shah, A.A., Li, M.Z., Xu, Q., Rosen, A., Casciola-Rosen, L., and Elledge, S.J. (2016). Systematic autoantigen analysis identifies a distinct subtype of scleroderma with coincident cancer. *Proc. Natl. Acad. Sci. USA* 113, E7526–E7534.
69. Rubtsov, A.V., Rubtsova, K., Fischer, A., Meehan, R.T., Gillis, J.Z., Kappler, J.W., and Marrack, P. (2011). Toll-like receptor 7 (TLR7)-driven accumulation of a novel CD11c<sup>+</sup> B-cell population is important for the development of autoimmunity. *Blood* 118, 1305–1315.
70. Brown, G.J., Cañete, P.F., Wang, H., Medhavy, A., Bones, J., Roco, J.A., He, Y., Qin, Y., Cappello, J., Ellyard, J.I., et al. (2022). TLR7 gain-of-function genetic variation causes human lupus. *Nature* 605, 349–356.
71. Cancro, M.P. (2020). Age-Associated B Cells. *Annu. Rev. Immunol.* 38, 315–340.
72. Ricker, E., Manni, M., Flores-Castro, D., Jenkins, D., Gupta, S., Rivera-Correa, J., Meng, W., Rosenfeld, A.M., Pannellini, T., Bachu, M., et al. (2021). Altered function and differentiation of age-associated B cells contribute to the female bias in lupus mice. *Nat. Commun.* 12, 4813.
73. Gödecke, N., Zha, L., Spencer, S., Behme, S., Riemer, P., Rehli, M., Hauser, H., and Wirth, D. (2017). Controlled re-activation of epigenetically silenced Tet promoter-driven transgene expression by targeted demethylation. *Nucleic Acids Res.* 45, e147.
74. Oyer, J.A., Chu, A., Brar, S., and Turker, M.S. (2009). Aberrant epigenetic silencing is triggered by a transient reduction in gene expression. *PLoS One* 4, e4832.
75. Kues, W.A., Schwitzer, R., Wirth, D., Verhoeven, E., Lemme, E., Herrmann, D., Barg-Kues, B., Hauser, H., Wonigeit, K., and Niemann, H. (2006). Epigenetic silencing and tissue independent expression of a novel tetracycline inducible system in double-transgenic pigs. *FASEB J.* 20, 1200–1202.
76. Pankiewicz, R., Karlen, Y., Imhof, M.O., and Mermod, N. (2005). Reversal of the silencing of tetracycline-controlled genes requires the coordinate action of distinctly acting transcription factors. *J. Gene Med.* 7, 117–132.
77. Dobin, A., and Gingeras, T.R. (2015). Mapping RNA-seq reads with STAR. *Curr. Protoc. Bioinformatics* 51, 11.14.1–11.14.19.
78. Li, B., and Dewey, C.N. (2011). RSEM: accurate transcript quantification from RNA-Seq data with or without a reference genome. *BMC Bioinformatics* 12, 323.
79. Langmead, B., and Salzberg, S.L. (2012). Fast gapped-read alignment with Bowtie 2. *Nat. Methods* 9, 357–359.
80. Li, H., Handsaker, B., Wysoker, A., Fennell, T., Ruan, J., Homer, N., Marth, G., Abecasis, G., and Durbin, R.; 1000 Genome Project Data Processing Subgroup (2009). The Sequence Alignment/Map format and SAMtools. *Bioinformatics* 25, 2078–2079.
81. Zhang, Y., Liu, T., Meyer, C.A., Eeckhoutte, J., Johnson, D.S., Bernstein, B.E., Nusbaum, C., Myers, R.M., Brown, M., Li, W., et al. (2008). Model-based analysis of ChIP-Seq (MACS). *Genome Biol.* 9, R137.
82. Love, M.I., Huber, W., and Anders, S. (2014). Moderated estimation of fold change and dispersion for RNA-seq data with DESeq2. *Genome Biol.* 15, 550.
83. Raudvere, U., Kolberg, L., Kuzmin, I., Arak, T., Adler, P., Peterson, H., and Vilo, J. (2019). g:Profiler: a web server for functional enrichment analysis and conversions of gene lists (2019 update). *Nucleic Acids Res.* 47, W191–W198.
84. Hao, Y., Hao, S., Andersen-Nissen, E., Mauck, W.M., 3rd, Zheng, S., Butler, A., Lee, M.J., Wilk, A.J., Darby, C., Zager, M., et al. (2021). Integrated analysis of multimodal single-cell data. *Cell* 184, 3573–3587.e29.
85. Granja, J.M., Corces, M.R., Pierce, S.E., Bagdatli, S.T., Choudhry, H., Chang, H.Y., and Greenleaf, W.J. (2021). ArchR is a scalable software package for integrative single-cell chromatin accessibility analysis. *Nat. Genet.* 53, 403–411.
86. Beard, C., Hochedlinger, K., Plath, K., Wutz, A., and Jaenisch, R. (2006). Efficient method to generate single-copy transgenic mice by site-specific integration in embryonic stem cells. *Genesis* 44, 23–28.
87. Ohhata, T., Senner, C.E., Hemberger, M., and Wutz, A. (2011). Lineage-specific function of the noncoding Tsix RNA for Xist repression and Xi reactivation in mice. *Genes Dev.* 25, 1702–1715.
88. Savarese, F., Flahndorfer, K., Jaenisch, R., Busslinger, M., and Wutz, A. (2006). Hematopoietic precursor cells transiently reestablish permissiveness for X inactivation. *Mol. Cell. Biol.* 26, 7167–7177.
89. Fiorentino, D.F., Mecoli, C.A., Rosen, M.C., Chung, L.S., Christopher-Stine, L., Rosen, A., and Casciola-Rosen, L. (2022). Immune responses to CCAR1 and other dermatomyositis autoantigens are associated with attenuated cancer emergence. *J. Clin. Invest.* 132, e150201.
90. Lundberg, I.E., Tjärnlund, A., Bottai, M., Werth, V.P., Pilkington, C., de Visser, M., Alfredsson, L., Amato, A.A., Barohn, R.J., Liang, M.H., et al. (2017). 2017 European League Against Rheumatism/American College of Rheumatology Classification Criteria for Adult and Juvenile Idiopathic Inflammatory Myopathies and Their Major Subgroups. *Arthritis Rheumatol.* 69, 2271–2282.
91. Fiorentino, D.F., Gutierrez-Alamillo, L., Hines, D., Yang, Q., and Casciola-Rosen, L. (2019). Distinct dermatomyositis populations are detected with different autoantibody assay platforms. *Clin. Exp. Rheumatol.* 37, 1048–1051.
92. Hochberg, M.C. (1997). Updating the American College of Rheumatology revised criteria for the classification of systemic lupus erythematosus. *Arthritis Rheum.* 40, 1725.
93. Petri, M., Orbai, A.M., Alarcón, G.S., Gordon, C., Merrill, J.T., Fortin, P.R., Bruce, I.N., Isenberg, D., Wallace, D.J., Nived, O., et al. (2012). Derivation and validation of the Systemic Lupus International Collaborating Clinics classification criteria for systemic lupus erythematosus. *Arthritis Rheum.* 64, 2677–2686.
94. Corces, M.R., Trevino, A.E., Hamilton, E.G., Greenside, P.G., Sinnott-Armstrong, N.A., Vesuna, S., Satpathy, A.T., Rubin, A.J., Montine, K.S., Wu, B., et al. (2017). An improved ATAC-seq protocol reduces background and enables interrogation of frozen tissues. *Nat. Methods* 14, 959–962.
95. Quinlan, A.R., and Hall, I.M. (2010). BEDTools: a flexible suite of utilities for comparing genomic features. *Bioinformatics* 26, 841–842.

96. Balboni, I., Chan, S.M., Kattah, M., Tenenbaum, J.D., Butte, A.J., and Utz, P.J. (2006). Multiplexed protein array platforms for analysis of autoimmune diseases. *Annu. Rev. Immunol.* *24*, 391–418.
97. Thibault, D.L., Graham, K.L., Lee, L.Y., Balboni, I., Hertzog, P.J., and Utz, P.J. (2009). Type I interferon receptor controls B-cell expression of nucleic acid-sensing Toll-like receptors and autoantibody production in a murine model of lupus. *Arthritis Res. Ther.* *11*, R112.
98. Nilsson, P., Paavilainen, L., Larsson, K., Ödler, J., Sundberg, M., Andersson, A.C., Kampf, C., Persson, A., Al-Khalili Szeghyarto, C.A.-K., Ottosson, J., et al. (2005). Towards a human proteome atlas: High-throughput generation of mono-specific antibodies for tissue profiling. *Proteomics* *5*, 4327–4337.
99. Tegel, H., Steen, J., Konrad, A., Nikdin, H., Pettersson, K., Stenvall, M., Tourle, S., Wrethagen, U., Xu, L., Yderland, L., et al. (2009). High-throughput protein production – Lessons from scaling up from 10 to 288 recombinant proteins per week. *Biotechnol. J.* *4*, 51–57.
100. Neiman, M., Hellström, C., Just, D., Mattsson, C., Fagerberg, L., Schuppe-Koistinen, I., Gummesson, A., Bergström, G., Kallioniemi, O., Achour, A., et al. (2019). Individual and stable autoantibody repertoires in healthy individuals. *Autoimmunity* *52*, 1–11.
101. Wang, D., Yang, L., Zhang, P., LaBaer, J., Hermjakob, H., Li, D., and Yu, X. (2017). AAgAtlas 1.0: a human autoantigen database. *Nucleic Acids Res.* *45*, D769–D776. <https://doi.org/10.1093/nar/gkw946>.
102. Suhas, S., Nathaniel, G.H., Liang, Z., Dahlgren, M.K., Junbong, J., Senbao, L., Benjamin, C.N., Cori, A.P., Xi, P., Mohamed, Y.E., et al. (2022). Unravelling psychiatric heterogeneity and predicting suicide attempts in women with trauma-related dissociation using artificial intelligence. *European Journal of Psychotraumatology* *13*, 2143693. <https://doi.org/10.1080/20008066.2022.2143693>.

## STAR★METHODS

### KEY RESOURCES TABLE

REAGENT or RESOURCE	SOURCE	IDENTIFIER
<b>Antibodies</b>		
7-AAD	BD Biosciences	Cat # 559925, RRID:AB_2869266
FITC anti-mouse CD4 (clone GK1.5)	BioLegend	Cat # 100406, RRID:AB_312690
TruStain FcX PLUS (anti-mouse CD16/32, clone S17011E)	BioLegend	Cat # 156604, RRID:AB_2783137
APC anti-mouse CD45 (clone 30-F11)	BioLegend	Cat # 103112, RRID:AB_312977
Mouse Xist Stellaris® FISH Probes with Quasar® 570 Dye	LGC Biosearch Technologies	SMF-3011-1, RRID: AB_3076254
R-Phycoerythrin labelled Goat anti-Human IgG Fc	Invitrogen	12-4998-82; RRID: AB_465926
<b>Biological samples</b>		
Human whole blood (healthy control serum)	Stanford Blood Center	<a href="https://stanfordbloodcenter.org/products-and-services/blood-products/">https://stanfordbloodcenter.org/products-and-services/blood-products/</a>
SLE patient sera	This paper; Johns Hopkins	NA
DM patient sera	This paper; Stanford University	NA
SSc patient sera	This paper; Johns Hopkins, Stanford University	NA
<b>Chemicals, peptides, and recombinant proteins</b>		
Pristane	Sigma-Aldrich	P9622-10X1ML
PBS 1x	Thermo Fisher Scientific	Cat # 10010049
Doxycycline hyclate	Sigma-Aldrich	D9891-5G
DNase I	Thermo Fisher Scientific	Cat# 18068015
O.C.T. Compound	Tissue-Tek	Cat# 4583
Fisherbrand™ Superfrost™ Plus Microscope Slides	Fisher Scientific	Cat# 12-550-15
Paraformaldehyde	Fisher Scientific	Cat# 50-980-487
TritonX-100	Acros Organics	AC327371000
Ethanol	Gold Shield	Cat# 412804
Stellaris® RNA FISH Wash Buffer A	LGC Biosearch Technologies	SMF-WA1-60
Stellaris® RNA FISH Hybridization Buffer	LGC Biosearch Technologies	SMF-HB1-10
VECTASHIELD Mounting Medium with DAPI	Vector Laboratories	H-1200
VWR® Micro Cover Glasses	VWR	48366-227
HypoThermosol FRS	BioLifeSolutions	Cat# 101102
CellTrics® Disposable Cell Strainers	Sysmex	04-004-2327
eBioscience™ 1X RBC Lysis Buffer	Thermo Fisher Scientific	Cat# 00-4333-57
BAMBANKER	Wako	Cat# 203-14681
Fetal Bovine Serum	Thermo Fisher Scientific	A3160502
Protector RNase Inhibitor	Sigma-Aldrich	Cat# 3335399001
<b>Critical commercial assays</b>		
EasySep Mouse CD4+ T cell Isolation Kit	STEMCELL Technologies	Cat# 19852
Mouse Anti-Nuclear Antibody Kit	MyBioSource.com	MBS731183
RNeasy Plus Mini Kit	Qiagen	Cat# 74136
High-Capacity cDNA Reverse Transcription Kit	Applied Biosystems	Cat# 4368814

(Continued on next page)

<i>Continued</i>		
REAGENT or RESOURCE	SOURCE	IDENTIFIER
TruSeq® Stranded mRNA Library Prep	Illumina	Cat# 20020594
Chromium Single Cell Multiome ATAC + Gene Expression Reagent Bundle	10x Genomics	PN-1000283
Chromium Next GEM Chip J Single Cell Kit	10x Genomics	PN-1000234
Single Index Kit N Set A, 96 rxns	10x Genomics	PN-1000212
Dual Index Kit TT Set A, 96 rxns	10x Genomics	PN-1000215
<b>Deposited data</b>		
Raw and processed sequencing data (single cell)	This paper	GEO: GSE249830
Raw and processed bulk ATAC-seq data	This paper	GEO: GSE249830
Raw and processed bulk RNA-seq data	This paper	GEO: GSE249830
Raw and processed SLE antigen array data	This paper	<a href="#">Table S3</a>
Raw and processed XIST antigen array data (patients)	This paper	<a href="#">Table S4</a>
Raw and processed XIST antigen array data (mouse)	This paper	<a href="#">Table S6</a>
<b>Experimental models: Organisms/strains</b>		
SJL/J mouse	Jackson Laboratories	Strain# 000686; RRID:IMSR_JAX:000686
C57BL6/J mouse	Jackson Laboratories	Strain# 000664; RRID:IMSR_JAX:000664
ΔRepA-Xist transgenic mouse	This paper	Anton Wutz
<b>Oligonucleotides</b>		
Mouse Xist Forward (RT-aPCR) GACAACAATGGGAGCTGGTT	Elim Biopharmaceuticals, Inc.	Custom Oligos
Mouse Xist Reverse (RT-aPCR) GCAACCCAGCAATAGTCAT	Elim Biopharmaceuticals, Inc.	Custom Oligos
Mouse GAPDH Forward (RT-aPCR) TGTGCAGTGCCAGCCTCGTC	Elim Biopharmaceuticals, Inc.	Custom Oligos
Mouse GAPDH Reverse (RT-aPCR) TGCCACTGCAAATGGCAGCC	Elim Biopharmaceuticals, Inc.	Custom Oligos
Neomycin Forward (genotyping) AGGATCTCCTGTCTCATCTCACCTT GCTCCTG	Elim Biopharmaceuticals, Inc.	Custom Oligos
Neomycin Reverse (genotyping) AAGAAGCTCGTCAAGAAGGCGAT AGAAGGCG	Elim Biopharmaceuticals, Inc.	Custom Oligos
CMV (genotyping, Forward) GCTGGTTTAGTGAACCGTCAG	Elim Biopharmaceuticals, Inc.	Custom Oligos
Mouse Xist (genotyping, Reverse) ACAAAGATTGGGCTGTCGAG	Elim Biopharmaceuticals, Inc.	Custom Oligos
<b>Software and algorithms</b>		
Cellranger	10x Genomics	<a href="https://support.10xgenomics.com/single-cell-gene-expression/software/overview/welcome">https://support.10xgenomics.com/single-cell-gene-expression/software/overview/welcome</a>
Prism	Graphpad	<a href="https://www.graphpad.com/scientific-software/prism/">https://www.graphpad.com/scientific-software/prism/</a>
CIBERSORT	Newman et al. <sup>28</sup>	<a href="https://cibersortx.stanford.edu/cshome.php">https://cibersortx.stanford.edu/cshome.php</a>
STAR	Dobin and Gingeras <sup>77</sup>	<a href="https://github.com/alexdobin/STAR">https://github.com/alexdobin/STAR</a>
RSEM	Li and Dewey <sup>78</sup>	<a href="https://github.com/deweylab/RSEM">https://github.com/deweylab/RSEM</a>
Bowtie2	Langmead and Salzberg <sup>79</sup>	<a href="http://bowtie-bio.sourceforge.net/bowtie2/index.shtml">http://bowtie-bio.sourceforge.net/bowtie2/index.shtml</a>

(Continued on next page)

**Continued**

REAGENT or RESOURCE	SOURCE	IDENTIFIER
Samtools	Li et al. <sup>80</sup>	<a href="http://www.htslib.org/">http://www.htslib.org/</a>
MACS2	Zhang et al. <sup>81</sup>	<a href="https://github.com/macs3-project/MACS">https://github.com/macs3-project/MACS</a>
DESeq2	Love et al. <sup>82</sup>	<a href="https://bioconductor.org/packages/release/bioc/html/DESeq2.html">https://bioconductor.org/packages/release/bioc/html/DESeq2.html</a>
g:profiler	Raudvere et al. <sup>83</sup>	<a href="https://biit.cs.ut.ee/gprofiler/gost">https://biit.cs.ut.ee/gprofiler/gost</a>
Seurat	Hao et al. <sup>84</sup>	<a href="https://satijalab.org/seurat/">https://satijalab.org/seurat/</a>
ArchR	Granja et al. <sup>85</sup>	<a href="https://www.archrproject.com/">https://www.archrproject.com/</a>

**RESOURCE AVAILABILITY**

**Lead contact**

Further information and requests for resources and reagents should be directed to and will be fulfilled by the lead contact, Howard Y. Chang ([howchang@stanford.edu](mailto:howchang@stanford.edu)).

**Materials availability**

All requests should be directed to the [lead contact](#), except  $\Delta$ RepA-Xist transgenic mice are available upon request with a completed Materials Transfer Agreement with Anton Wutz ([awutz@ethz.ch](mailto:awutz@ethz.ch)).

**Data and code availability**

- Bulk ATAC- and RNA-seq and single cell multiomic data have been deposited in the NCBI GEO database. Accession numbers can be found in the [key resources table](#). The autoantigen array raw data files are included in [supplemental information](#). Additional identifier information for deposited data can be found in the [key resources table](#).
- Analysis details are provided in [STAR Methods](#). No original code was generated in this paper.
- Additional information required to reanalyze the data reported in this paper is available from the [lead contact](#) upon request.

**EXPERIMENTAL MODELS AND STUDY PARTICIPANT DETAILS**

**Mouse Strains**

All mouse work was conducted under Stanford's approved animal protocol APLAC-14046. Wild-type C57BL/6J (000664) and SJL/J (000686) mice were purchased from Jackson Laboratories. Inducible  $\Delta$ RepA-Xist transgenic mice: A transgene of tetO linked to *Xist* cDNA deleted for the A repeat (SacII-XhoI is deleted, appx. 500nt) was targeted to the *Col1a1* locus on chromosome 11 in A9 129/B16 hybrid ES cells. To insert the  $\Delta$ RepA-Xist transgene, a homing cassette was first inserted into the 3'-region of *Col1a1* using homologous recombination. This homing cassette consisted of a hygromycin (pPGK-hygro-PA) resistance marker, a loxP recombinase site, and a truncated neomycin resistance gene (3'neo-PA). Subsequently, the pPGK-loxP- $\Delta$ RepA-Xist cDNA was inserted by Cre mediated recombination followed by G418 selection.<sup>18,86</sup> Transgenic mice were generated by injection of the modified ES cells into B16 8-cell embryos.<sup>87</sup> Resulting transgenic mice were crossed to a mouse line carrying the R26/N-*nlst*TA doxycycline regulated transactivator.<sup>87,88</sup> Mice carrying the tet-O- $\Delta$ RepA-Xist and rTA constructs were backcrossed into the C57BL/6J or SJL/J mice for multiple generations. Tail tips were collected from 5-7 female mice from each generation for speed congenics selection using Charles Rivers' MAX-BAX 384 SNP panel. The two females with the highest match in the desired background from each generation were selected as breeders. The tgXist-C57BL6/J mice used in this study are > 80% in the C57BL/6J background. The tgXist-SJL/J mice are > 99.99% in the SJL/J strain background. Mice were genotyped for both the Neomycin resistant cassette and from the CMV promoter into the truncated *Xist* transgene. Studies in the SJL/J background used both mice heterozygous for tgXist and wild-type littermates while studies involving SJL/J mice while wild-type control C57BL/6J mice were obtained from Jackson Laboratories. Genotyping primers are listed in the [key resources table](#).

**Clinical Cohorts**

All human patient samples were de-identified in this study and obtained under the respective institutions' IRB-approved protocols.

The biological sex of human serum samples used in this study is indicated in the text and raw data tables in [Table S4](#) in the "SAMPLES" description sheet. All patients were adults. Information regarding age, ancestry, race, ethnicity, and socioeconomic status were not provided in the de-identified clinical patients to the Lead Author in this study and so were not included in the analysis. Due to the small number "n" of male patients, sex was not a separately analyzed variable due to lack of statistical power. Analysis was, instead, separated into disease groups.

### General Population

Donated whole blood from a total of 9 male and 8 female donors were obtained from the Stanford Blood Bank following IRB-approved protocols (IRB #13942) with confirmed assent for use in research. Serum was collected as described above in the mouse serum section and frozen in  $-80^{\circ}\text{C}$  for long-term storage. During data analysis, 1 of the 9 male samples was filtered out for high IgG background.

### Dermatomyositis (Stanford)

Serum from 1 male and 3 female dermatomyositis patients were used in this study. All samples were collected from patients seen at the Stanford outpatient clinics under an IRB-approved protocol (IRB #12047), and all patients provided informed consent to participate. The dermatomyositis cohort has been described previously.<sup>89</sup> All patients met probable or definite DM by 2017 ACR/EULAR IIM Classification Criteria.<sup>90</sup> All sera used in the study were also known to contain antibodies against TIF1- $\gamma$  which was assayed as previously described.<sup>91</sup>

### Systemic Sclerosis (Scleroderma, Stanford)

Serum from 24 patients (2 male and 22 female) with systemic sclerosis (SSc) were included in this study from the Stanford cohort. All samples were collected from patients seen at the Stanford outpatient clinics under an IRB-approved protocol (IRB #12047), and all patients provided informed consent to participate. All patients fulfilled 2013 ACR/EULAR classification criteria for SSc. Twelve patients had diffuse and 12 had limited cutaneous SSc. Seven patients had the Scl-70 antibody, 5 had the anti-centromere antibody, 2 patients had RNA polymerase III, 2 had nucleolar ANA, 2 had PM/Scl, and 1 had U1RNP, with the remainder having positive ANA but no known SSc-specific autoantibody.

### Systemic Sclerosis (Scleroderma, Johns Hopkins)

Samples were previously collected and stored at  $-80^{\circ}\text{C}$  as part of the Hopkins Scleroderma Center cohort protocol (NA\_00039566). Serum from 9 males and 31 females were shipped on dry ice to Stanford. Patients were enrolled in the IRB-approved Johns Hopkins Scleroderma Center Research Registry. Scleroderma participants in the registry meet at least one of the following criteria for systemic sclerosis: 1) 2013 ACR/EULAR classification criteria for scleroderma, 2) 1980 ACR classification criteria, 3) having at least 3 of 5 features of the CREST syndrome (calcinosis, Raynaud's phenomenon, esophageal dysmotility, sclerodactyly, telangiectasia), or 4) having definite Raynaud's phenomenon, abnormal nailfold capillaries and a scleroderma-specific autoantibody.

### Systemic Lupus Erythematosus (Johns Hopkins)

Patients provided written informed consent to participate in the Hopkins Lupus Cohort (IRB study number NA\_00039294). Blood was drawn at the time of a clinical blood draw, serum collected and kept in a  $-80$  freezer for long term storage. For this study, 40 serum samples (3 males and 37 females) were randomly selected from patients who were ever: 1) ANA positive with a titer of at least 1:320; and 2) positive to the dsDNA autoantigen. Patients enrolled in the Hopkins Lupus Cohort met either the revised American College of Rheumatology (ACR)<sup>92</sup> or Systemic Lupus International Collaborating Clinics (SLICC)<sup>93</sup> criteria for SLE. Samples were shipped on dry ice to Stanford and stored at  $-80^{\circ}\text{C}$ .

## METHOD DETAILS

### Induction and evaluation of pristane-induced SLE in mice

#### Pristane-induction of SLE

Wild-type and *tg-Xist* mice were injected with a one-time injection of 0.5 mL of pristane (Sigma-Aldrich, P9622-10X1ML) at 8-10 weeks old (SJL/J strain) or 12-14 weeks old (C57BL/6J studies). Control animals were injected with PBS 1x (Thermo Fisher Scientific, 10010049).

#### Induction of transgene (*tgXist*)

Simultaneous to the injection date, doxycycline hyclate (Sigma-Aldrich, D9891-5G) was continuously administered at 0.2 g/mL in drinking water to select mice until the terminal timepoint.

For the *tgXist* expression validation studies, *tgXist*<sup>+/-</sup> and wild-type mice in the C57BL/6J strain were administered doxycycline for 2 weeks and tissues were harvested for qRT-PCR and FISH analysis.

#### *Xist* RT-qPCR

Mechanically dissociated thymus, spleen, kidney, and liver cells harvested from *tgXist*<sup>+/-</sup> and wild-type mice in the C57BL/6J were strained through a cell filter, pelleted, and frozen in RLT Buffer with 0.1% BME. RNA was extracted using the RNeasy Mini kit (Qiagen, 74106), genomic DNA was removed using amplification grade DNase I (Thermo Fisher Scientific, 18068015). RNA concentration was quantified on a Nanodrop. cDNA was made from 1  $\mu\text{g}$  of RNA/sample using the High-Capacity cDNA Reverse Transcription Kit (Applied Biosystems, 4368814). Each Ct value was measured using Lightcycler 480 (Roche) and each mean dCt was averaged from triplicate qRT-PCR reactions. Relative *Xist* RNA levels was calculated by ddCt method compared to GAPDH controls. Statistical significance was calculated using the Student's t-test. Primer sequences are listed in the [key resources table](#).

#### *Xist* FISH

Mice organs frozen in O.C.T. compound (Tissue-Tek, 4583) were sectioned on a cryostat to 15  $\mu\text{m}$  onto microscope slides (Fisher Scientific, 12-550-15). Sections were washed once with PBS 1x, fixed in 4% paraformaldehyde for 10 min at room temperature, washed twice with PBS 1x for 2-5 min each, then permeabilized on ice with ice cold 0.5% TritonX-100 in PBS for 10 min. Slides were then rinsed once with PBS and dehydrated sequentially in 70%, 90% and 100% Ethanol (Gold Shield, 412804) for 5 minutes

each. Sectioned slides were then allowed to air dry before immersion in freshly made Stellaris® RNA FISH Wash Buffer A (SMF-WA1-60) for 2-5 minutes at room temperature. Sections were then hybridized overnight for 16-18 hours in the dark at 42C in 250 nM of Mouse Xist Stellaris® FISH Probes with Quasar® 570 Dye (LGC Biosearch Technologies, SMF-3011-1) in Stellaris® RNA FISH Hybridization Buffer (SMF-HB1-10). The next day, slides were incubated twice in Wash Buffer A for 30 minutes at 37C followed by immersion in Stellaris® RNA FISH Wash Buffer B for 2-5 minutes at 27C, mounted in VECTASHIELD Mounting Medium with DAPI (Vector Laboratories, H-1200) and sealed with cover glass (VWR, 48366-227) and nail polish clear coat. Sectioned organs were imaged on the Zeiss Observer Z.1 using the 63x oil objective, X-Cite Series120 laser, and AxioVision Rel. 4.8 software.

#### **Mouse sera collection**

Mice were sedated with isoflurane and retro-orbitally bled immediately prior to the injection and viably bled every 4 weeks until the terminal date. On the terminal date, blood was collected through cardiac puncture. Blood was allowed to clot for 2 hours at room temperature, then spun for 15 minutes at 1500xg at room temperature. Serum was immediately collected, flash-frozen on dry ice and stored at -80C.

#### **ANAb ELISA**

Serum ANAb levels were measured using the Mouse Anti-Nuclear Antibody Kit ([MyBioSource.com](https://www.mylabsci.com/), MBS731183) and assessed on an ELISA plate reader at an optical density of 450 nm. Titration curves and values were calculated using a Four Parameter Logistic Curve.

#### **Tissue collection and preparation of pristane-induced SLE studies**

Mice were euthanized by CO<sub>2</sub> asphyxiation and cardiac exsanguination at the terminal timepoints of 16- or 52-weeks post-injection. Terminal cardiac blood was aliquoted into EDTA tubes (400 ml per mouse) and Eppendorf tubes (for serum collection). Total body weights were obtained, and the following organs were weighed individually: thymus, heart, liver, spleen, testes. Gross necropsies were performed on all mice (Table S7). The caudate and papillary liver lobes, left kidney, one half of the thymus and one half of the spleen were dissected and placed on ice in HypoThermosol FRS (BioLifeSolutions, 101102) until all dissections concluded and were either mechanically dissociated using clean scalpels and syringes or frozen in O.C.T. Compound (Tissue-Tek, 4583) at -80C on the same day. The remaining tissues were immersion-fixed in 10% neutral buffered formalin for 72 hours for downstream histology analysis. Dissociated cells were passed through cell filters (Sysmex, 04-004-2327), pelleted at 300xg, incubated for 1 minute at room temperature in eBioscience™ 1X RBC Lysis Buffer (00-4333-57) to remove red blood cells, and quenched with 10x the volume of PBS 1X. For viable stocks, dissociated cells were frozen in BAMBANKER (Wako, #203-14681) and stored in liquid nitrogen.

#### **CD4+ isolation**

CD4+ cells were isolated from freshly dissociated mouse spleen using the EasySep Mouse CD4+ T cell Isolation Kit (STEMCELL Technologies, 19852). CD4+ cells were then immediately used for bulk ATAC-seq, frozen in RLT Buffer Plus, or viably frozen in BAMBANKER. A small aliquot of cells were stained in PBS 1x with the viability marker 7-AAD (BD Biosciences, 559925) and T-cell marker CD4 FITC (clone GK1.5, BioLegend, 100406) to assess purity and viability on a FACS analyzer.

#### **CD45+ isolation**

Viable cells frozen in BAMBANKER were thawed at 37C in a bead bath, resuspended in RPMI, and spun at 300xg to pellet and remove the buffer. Cells were incubated with TruStain FcX PLUS (anti-mouse CD16/32, clone S17011E, Biolegend, 156604) to block non-specific binding of immunoglobulin and stained with the pan-hematopoietic marker CD45 APC (clone 30-F11, BioLegend, 103112) and 7-AAD for viability. Viable CD45+ cells were sorted on the BD FACSAria II sorter using a 70 µm nozzle into chilled FBS (Thermo Fisher Scientific, A3160502) with 1% Protector RNase inhibitor (Sigma-Aldrich, 3335399001) in the Stanford Shared FACS Facility. Sorted cells were then immediately used to prepare sequencing libraries.

#### **Histopathology**

Formalin-fixed tissues were processed routinely, embedded in paraffin, sectioned at 5 µm, and stained with hematoxylin and eosin. All tissues were evaluated blindly by a board-certified veterinary pathologist (KMC). An ordinal histopathologic grading scale (score 0-4) was designed to evaluate glomerulonephritis, hepatic lipogranulomas, pulmonary lymphohistiocytic alveolitis, and splenic extramedullary hematopoiesis. A binary histopathologic grading scale (score 0 or 1) was used to evaluate for intra-abdominal lipogranuloma formation and ectopic lymphoid tissue, pulmonary hemorrhage, hemosiderosis, and/or vascular thrombosis, splenic lymphoid hyperplasia and plasmacytosis, and lymph node hyperplasia and medullary plasmacytosis. A total composite score was derived for each mouse. The Fisher's Exact Test was used to calculate significance between treatment groups. Due to facility and equipment difficulties during the COVID-19 pandemic, some mice are missing scores for kidney or spleen. Only mice with all organs correctly processed and assessed were used to calculate the composite score and included in the final analysis (shown in Figure 3). Complete scores for all SJL/J mice used in the pristane-induced lupus study can be found in the Table S7.

#### **Statistical Analysis of histopathology scores**

The Fisher's Exact Test was used to calculate significance between treatment groups in the histopathology studies. Because the lowest positive female control total body disease score was 10, we set 10 as the cutoff total body disease score to distinguish between low disease and high disease scores.

## Sequencing Library Preparation

### Bulk sequencing

ATAC-seq libraries of freshly isolated CD4<sup>+</sup> cells were prepared using the Omni-ATAC protocol.<sup>94</sup> RNA was extracted using the RNeasy Plus Mini Kit (Qiagen, 74136). TruSeq® Stranded mRNA Library Prep (Illumina, 20020594) was used to generate polyA-selected RNA-sequencing libraries, cleanup performed on magnets with AMPure XP beads (Beckman Coulter, A63880). The bulk ATAC-seq and RNA-seq libraries were sequenced with paired-end 75 bp read lengths on in the Stanford Functional Genomics Facility an Illumina HiSeq 4000 that was purchased with funds from NIH under award number S10OD018220.

### Single cell sequencing

The Chromium Single Cell Multiome ATAC + Gene Expression (10x Genomics) was used to prepare libraries for CD45<sup>+</sup> sorted cells with a target of 10,000 cells/sample. Libraries were sent to Novogene for Bioanalyzer trace quality control check and sequencing. Libraries were sequenced on the NovaSeq 6000 at a depth of 20,000 paired reads per cell for gene expression libraries and 25,000 paired reads per cell for ATAC libraries.

## Computational Analysis of Sequencing Libraries

### Bulk sequencing

The bulk RNA-seq data was aligned to mm10 using STAR.<sup>77</sup> The gene expression read counts was generated using RSEM.<sup>78</sup> The adaptor of paired-end ATAC-seq data was trimmed and aligned to mm10 genome using bowtie2.<sup>79</sup> The mitochondrial reads and reads with low alignment score (<10) were removed. The aligned sam files were converted to bam files and sorted by Samtools.<sup>80</sup> Picard was used to remove duplicate reads and MACS2<sup>81</sup> was used to call peaks. BEDtools<sup>95</sup> was used to generate read counts from called peaks. Each ATAC-seq peak was annotated by its nearby genes using GREAT under the basal plus extension default setting.

The raw bulk RNA-seq and ATAC-seq read counts were then normalized and analyzed using DESeq2.<sup>82</sup> The differentially expressed genes and ATAC-seq peaks were identified using the negative binomial models. Benjamini hochberg procedure was used to adjust for multiple hypothesis testing. Peaks with FDR < 0.2 and absolute fold change larger than 1.5 were selected as significant. Bioinformatics tool g:Profiler<sup>83</sup> was used for pathway enrichment analysis. CIBERSORT<sup>28</sup> was used to estimate the abundance of immune cells based on normalized RNA-seq data.

### Single cell multiomics sequencing

The single-cell paired RNA and ATAC-seq reads were aligned to the mm10 reference genome using cellranger-arc count (10x Genomics, version 2.0.1).

Gene expression data was filtered to include only barcodes that had nFeature > 500 and pct.mt < 12. Two female samples (F100 and F113) were excluded because, even after stringent filtering, cells from these samples had lower quality metrics than other samples. R v4.1.3 Seurat v4.1.1<sup>84</sup> and ggplot2 v3.3.6 were used for downstream analysis and visualization. After filtering, clustering and dimensionality reduction was performed using the top 10 principal components (dims=1:10) and a clustering resolution of 0.25. Differential gene expression analysis was performed using Seurat function "FindMarkers" with default settings.

Single cell ATAC data was processed with ArchR v1.0.1.<sup>85</sup> ATAC-seq data was subsetted using the subsetArchRProject function to include only cells with matched gene expression cell IDs and clustered at resolution=0.7 with default settings. Gene imputation features of defining cell type markers were visualized from the GeneScoreMatrix using default settings. Cellular subsets were subsequently subsetted and analyzed with getMarkerFeatures from the PeakMatrix using default settings and maxcells=5000 and k=1000.

### Calculation of Chr11 accessibility and gene expression

The aforementioned Chromium Single Cell Multiome ATAC + Gene Expression (10x Genomics) libraries were used in the analysis of Chr11 between the three treatment groups (Wt F+ Pristane, tgXist M + Pristane + Dox, and Wt M + Pristane + Dox).

### Chr11 track analysis

The bigwig files for each mouse treatment group were generated using the getGroupBW function in the archR package. Boxplots were visualized in the rtracklayer package in R using bigwig files containing normalized ATAC-seq counts. Genome position-wide scATAC track visualization was obtained using the plotBrowserTrack function in the archR package. The FindMarkers function in the Seurat package was used to identify the differential expressed genes between the pristane+dox treated groups: Wt M versus and tgXist M. A hypergeometric test was then applied to examine whether the genes on chr11 are more likely to be down regulated compared with the genome wide scale.

## SLE autoantigen Panel Array

### Assay

Mouse serum was assessed using the SLE autoantigen panel and array as previously described.<sup>36</sup> Serum from the baseline timepoint of 0 weeks (injection start) and terminal timepoints (16 weeks for SJL/J and 52 weeks for C57BL/6J strains) were run in the same assay (sample-matched). Serum was stored long-term at -80°C and prepared as previously described.<sup>36</sup> Raw MFI values and mouse serum sample information can be found in [Table S3](#).

### Analysis

Raw MFI scores were first normalized by subtracting the baseline value of bare bead, with a minimum differential limit set at 0 to account for values below baseline. The difference between terminal and baseline timepoints was then calculated using the normalized values, with a minimum differential limit set at 0 as “depletion” of autoantibodies is not expected to occur over time. Values were plotted in GraphPad Prism and the Wilcoxon Rank Sum Test was used to test for statistical significance. The Benjamini-Hochberg procedure was used to calculate FDR and correct for multiple comparisons.

### XIST Autoantigen Array

#### Autoantigen list

Available recombinant proteins were chosen from a set of XIST-associating proteins of interest from published XIST ChIRP datasets<sup>12,14</sup> at a stringency of  $\log_2(\text{EXP}/\text{RNAse}) > 1$  and peptide EXP Sum  $\geq 10$ . Due to the limited availability of recombinant proteins, this criteria is less stringent than that used for the bibliomics analysis (Table S1, Figure S1) in order to include a larger set of XIST-associating proteins of interest. Autoantigens clinically used to screen for DM,<sup>53</sup> SLE or SSC<sup>96,97</sup> were included as positive controls. 16 exploratory proteins were included from unpublished XIST ChIRP-MS lists. Each protein was represented by one or more protein fragments (20-151 amino acids long) produced within the Human Protein Atlas project (<https://www.proteinatlas.org/>).<sup>98,99</sup> The full list of autoantigens and their categorization can be found in Tables S4 and S6.

#### Sample preparation

25  $\mu\text{L}$  of serum per sample were aliquoted in a pre-determined randomized order onto 96-well plates (Thermo Fisher Scientific, AB800150) with mouse and human samples on separate plates. Thermal sealed plates were shipped on dry ice to SciLifeLab in Sweden and stored at  $-80\text{C}$  upon arrival.

#### Suspension Bead Array Assay (SciLifeLab)

The antigens were immobilized on color coded magnetic beads (MagPlex, Luminex Corp., Austin, TX) and the assay was run as previously described, with minor alterations.<sup>100</sup> The samples were diluted directly before running the assay, prior to adding the secondary antibody the beads incubated for 10 minutes in 0.2% paraformaldehyde to fixate any bound antibodies, and the secondary antibody used was R-Phycoerythrin labelled Goat anti-Human IgG Fc (eBioscience™; 12-4998-82, Invitrogen).

#### Data handling and analysis

All data processing from the suspension bead array was performed using R version 4.1.1. Antigen specific background was adjusted for by centering and scaling the 10<sup>th</sup> percentile of the mean fluorescence intensity (MFI) value for each antigen to a common value (10<sup>th</sup> percentile of the whole dataset). The antigen percentile adjusted MFI values were transformed per sample into the number of “median absolute deviations” (MADs) around the sample, represented as:  $\text{MADs}_{\text{ag, sample}} = (\text{MFI}_{\text{adj, sample}} - \text{median}_{\text{sample}}) / \text{MAD}_{\text{sample}}$ . Raw MFI values can be found in Tables S4 and S6.

For the general population and patient disease comparison analyses, the difference in reactivity was calculated as the difference between the mean of the MAD scores of the comparison groups and significance was calculated using the Student’s T-Test. To remove far-lying outliers, MAD scores were first “trimmed” to quantile (0.1, 0.9). Since each protein often contained multiple protein fragments in the assay, the list was next filtered to remove duplicate counts and generate a unique list of reactive proteins. The reactive protein lists were then compared between patient disease groups (Figures 6D and 6E; Table S5).

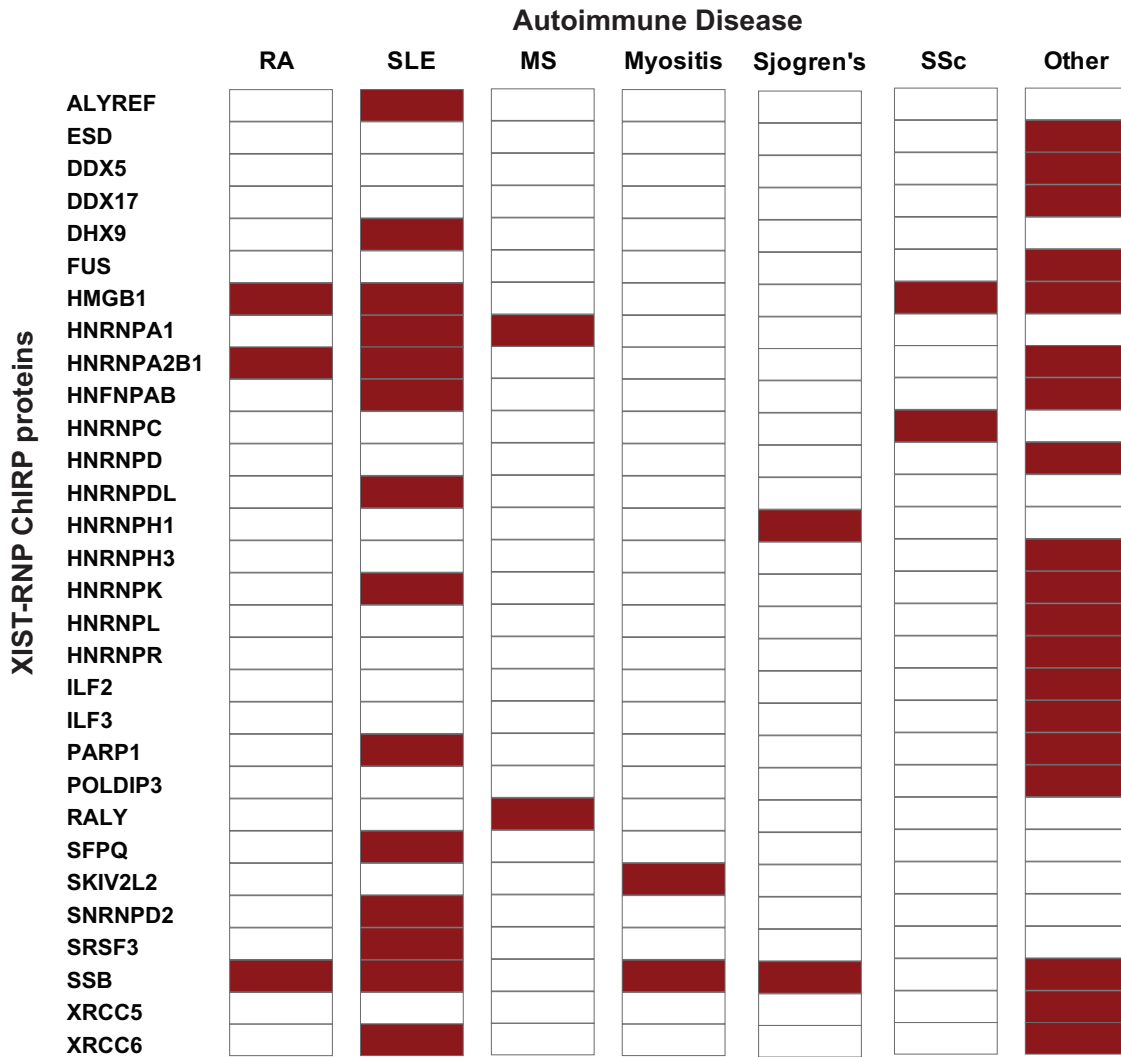
#### Selection of enriched proteins

To find shared reactive proteins in two heterogeneous datasets (pristane-induced SLE mouse and autoimmune disease patients), the difference in MAD scores was calculated in patients as the difference between SLE patient reactivity and the general population (healthy control) and in mice as the difference between 16 weeks and 0 weeks (treatment start baseline) for each group. Protein fragments were considered reactive in patients if  $\text{MADs}_{\text{diff}} > 0$  in the quantile “trimmed” set and  $\text{MADs}_{\text{diff}} > 2.5$  in the raw datasets. Protein fragments were considered reactive in mice if  $\text{MADs}_{\text{diff}} > 2.5$  between 16 and 0 weeks. Since each protein often contained multiple protein fragments in the assay, the list was next filtered to remove duplicate counts and generate a unique list reactive proteins. The enriched protein lists were then compared between the pristane-induced SLE mouse groups and SLE patients (Table S5).

## QUANTIFICATION AND STATISTICAL ANALYSES

All statistical analysis and quantification were conducted in R or GraphPad Prism. Three standardized comparisons are made across mouse cohorts in Figures 3, 4, 5, and 7: (1) WT female mice treated with pristane vs. WT male mice treated with pristane (positive vs. negative control); (2) tgXist male mice +Dox + pristane vs. WT male mice + pristane (test vs. negative control); (3) WT female mice + pristane vs. tgXist male mice + Dox + pristane (positive control vs. test). The p-values are indicated on the figures; multiple hypothesis testing is controlled for using the Benjamini-Hochberg method to estimate false discovery rate (FDR). All indicated significant p-values have a  $\text{FDR} < 0.05$  accounting for multiple hypothesis testing. Non-significant comparisons, including those rejected based on FDR, are indicated with “NS” on the figure. Figure legends state the statistical details of the experiments and assays, including exact “n” values, statistical tests, comparisons, and cutoffs specifically used in each figure.

# Supplemental figures



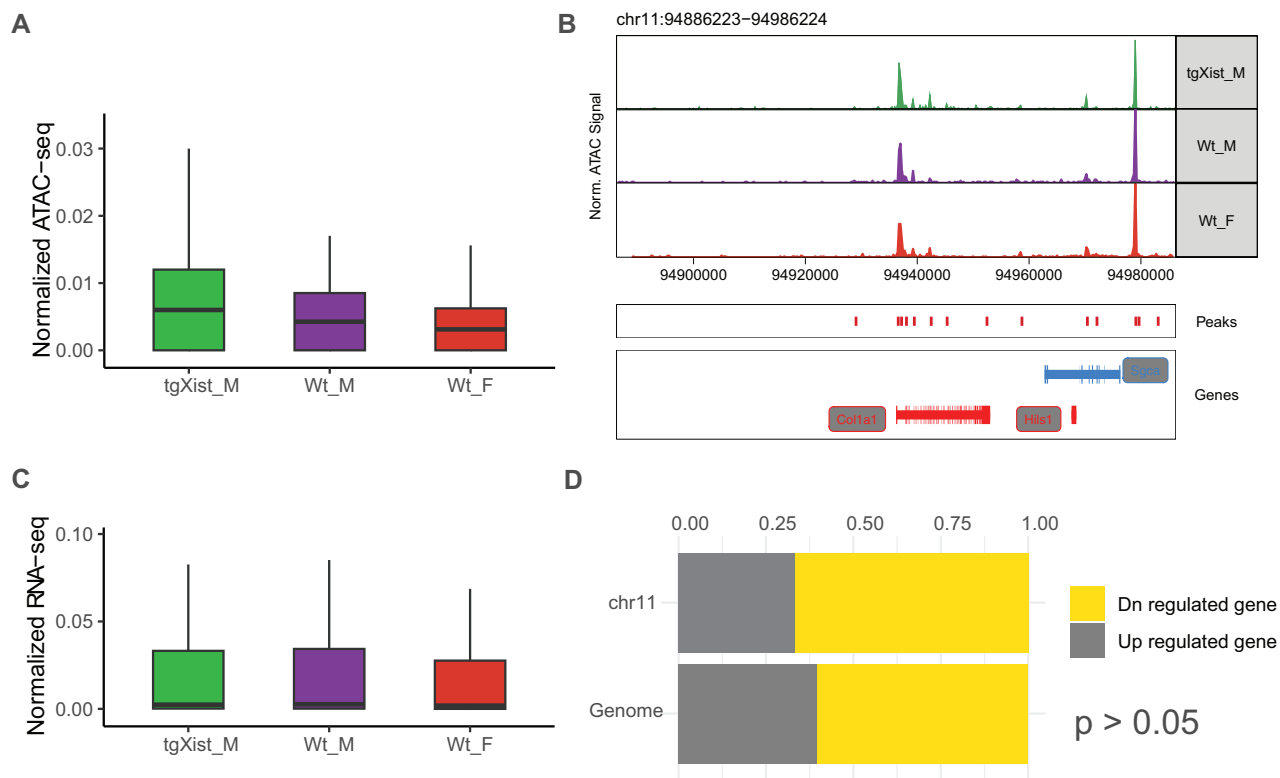


**Figure S2. Chromosome-wide comparison of tgXist transgene insertion in Col1A1 safe harbor locus on chr11, related to Figures 1 and 4**

(A) Chromatin accessibility at chr11 assessed using single-cell ATAC-seq data.

(B) ATAC-seq accessibility tracks in the Col1A1 insertion locus.

(C) Gene expression profile at chr11 using single-cell RNA-seq data.

(D) Fraction of upregulated and downregulated genes on chr11 and genome-wide, comparing tgXist males and WT male mice. All plot values obtained from single-cell multiomic data normalized to sequencing depth from pristane-treated SJL/J mice: number of tgXist M + Dox + pristane = 8, WT M + Dox + pristane = 3, WT F + pristane = 2. Significance was calculated using Fisher's exact test.

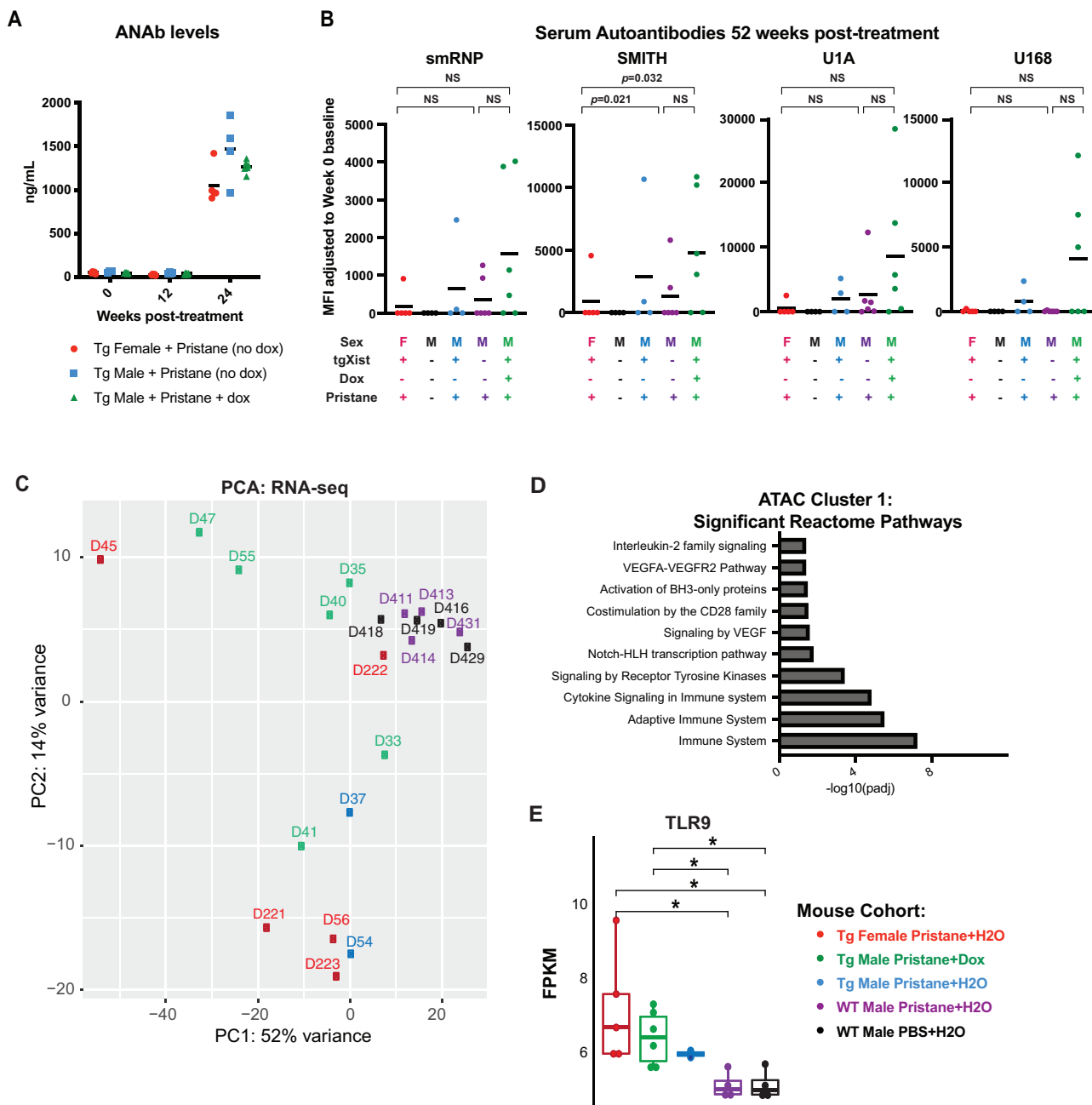


**Figure S3. Serum autoantibodies and ATAC-seq and RNA-seq from pristane-treated mice in the C57BL/6J background, related to Figure 2**

(A) ELISA of serum ANAb levels, number of tgXist female = 5, tgXist male (no Dox) = 4, tgXist male + Dox = 6. ANAb of WT male animals were done but did not meet quality control standards and therefore not shown.

(B) Median fluorescence intensity (MFI) of serum reactivity to representative autoantigens, using a bead-based lupus antigen array after 52 weeks of treatment. (A and B) From left to right tgXist female control to tgXist male test, number of animals in serum studies: n = 5, n = 4, n = 4, n = 6, n = 6. (A and B) Statistical significance calculated with Wilcoxon rank-sum test, FDR < 0.05.

(C) PCA plots of RNA-seq libraries of all five mouse cohorts.

(D) Top 15 differential reactomes associated with ATAC-seq cluster 1 genomic regions.

(E) Comparison of fragments per-kilobase per-million mapped fragments (FPKM) in the TLR9 gene region. Significance calculated using the Student's t test. \* indicates  $p < 0.05$ . (C–E) Number of mice used: WT F+ pristane = 5, tgXist M + pristane + Dox = 6, tgXist M + pristane = 2, WT M + pristane = 4, WT M mock treatment = 4.

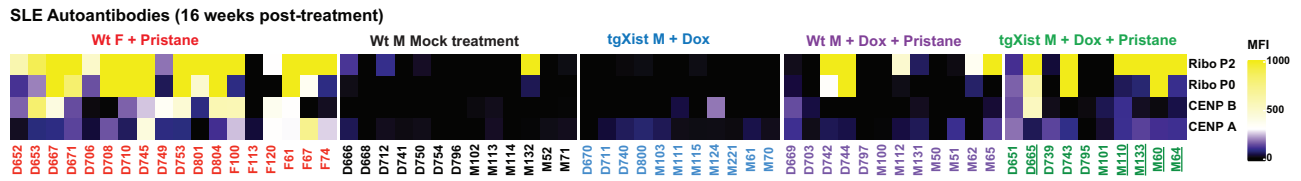
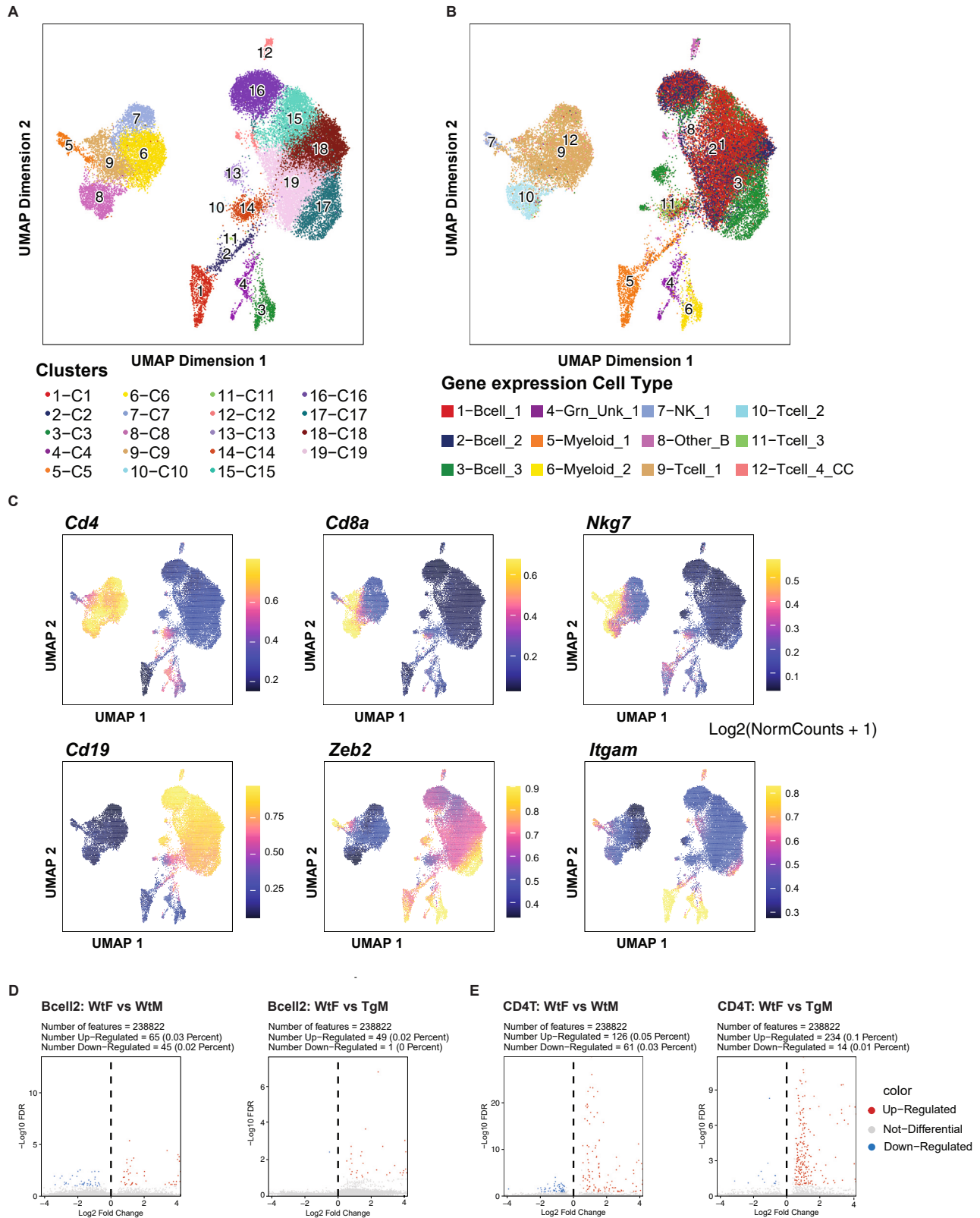


**Figure S4. Serum autoantibodies in pristane-treated mice in the SJL/J background, related to Figure 3**

Heatmap of the MFI values at 16 weeks (normalized to 0 weeks) of autoantigens displayed in Figure 3F. Color labels correspond to the mouse treatment group. Each row is an autoantibody; each column is an individual mouse. In the tgXist M + Dox + pristane group, male mice with female-level total pathology score (score > 10 in Figure 3E) are shown with underlined sample ID numbers. However, the autoantibody response is heterogeneous; the four antibodies as a group are not significantly different between tgXist M + Dox + pristane vs. WT M + Dox + pristane. Number of mouse serum samples, listed from left to right: wild-type female + pristane = 18, wild-type male negative control = 13, tgXist male + Dox (tgXist) control = 11, wild-type male treatment = 12, tgXist male treatment = 10.

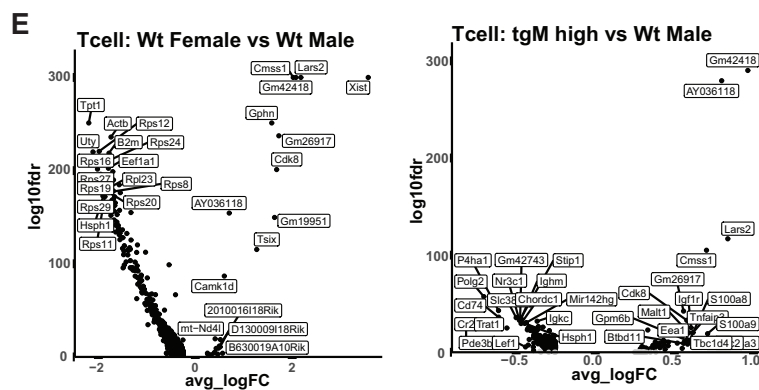
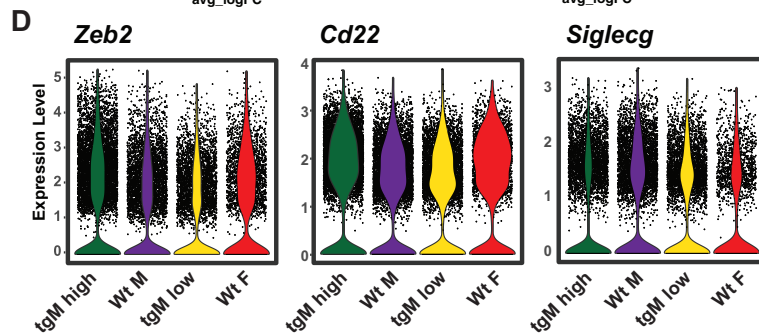
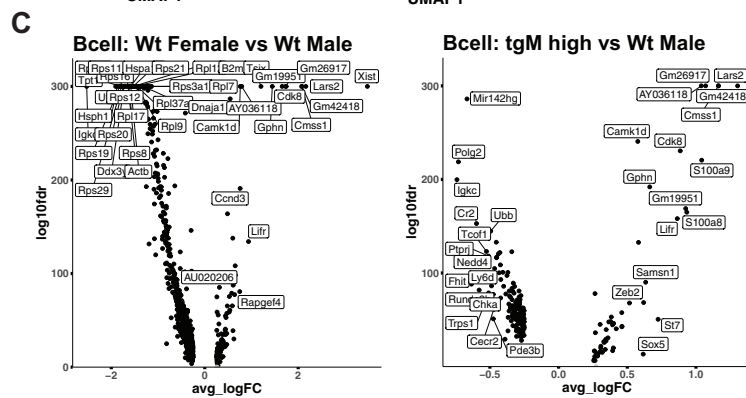
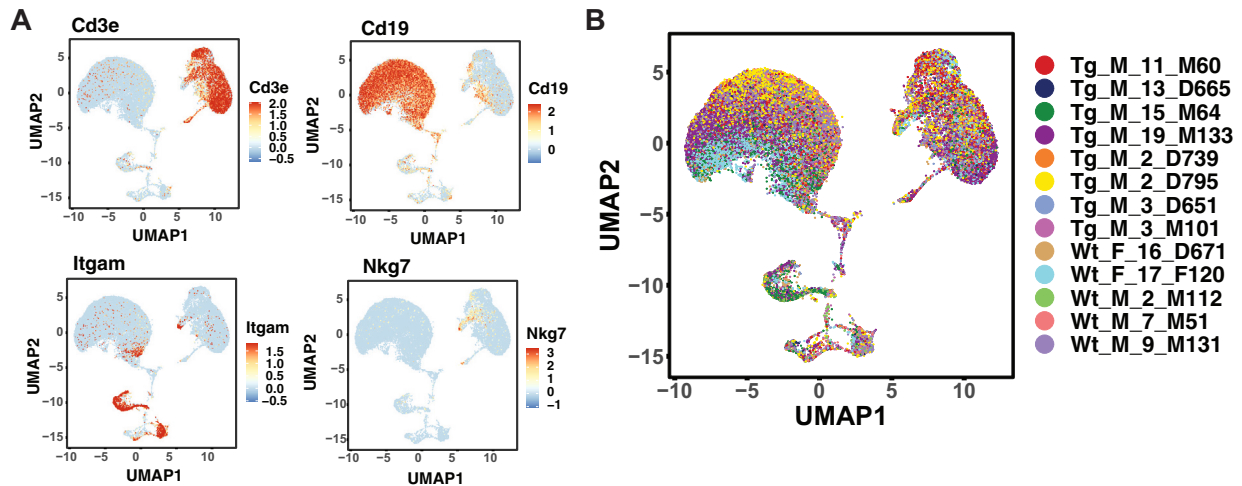


(legend on next page)

---

**Figure S5. Splenic CD45+ hematopoietic cells single-cell ATAC from pristane-induced SLE mice of the SJL/J strain, related to Figure 4**

(A and B) (A) Original single-cell ATAC clusters and (B) matched single-cell gene expression-determined cell identities displayed on the single-cell ATAC UMAP. (C) Localization of defining markers, calculated by imputation from ATAC data, used to determine cell-type identity. Imputation scale  $\log_2(\text{NormCounts} + 1)$ . (D) Pairwise comparison metrics of differential peaks between WT female (positive disease control) and the low disease male control groups (WT male and tgXist male low disease) across the four main cellular subsets shown for features  $\text{FDR} \leq 0.1$  and  $\log_2\text{FC} \geq 0.5$ . Pristane-treated mouse groups shown: tgXist male, disease high (n = 4); tgXist male, disease low (n = 4); wild-type male (n = 3); and wild-type female (n = 2). Significance was calculated using the Wilcoxon rank-sum test.



---

**Figure S6. Splenic CD45<sup>+</sup> hematopoietic cells single-cell gene expression from pristane-induced SLE mice of the SJL/J strain, related to Figure 5**

- (A) Localization of defining expression markers used to determine immune cell-type identities of UMAP clusters.
- (B) Individual mice displayed on the single-cell gene expression clustering UMAP. Individual mouse labels displayed as follows: transgenic status\_sex\_total disease damage score\_mouse colony ID.
- (C) Volcano plots of differentially expressed B cell cluster genes comparing tgXist male high disease and WT female with WT male.
- (D) Representative violin plots of B cell marker genes from the combined B cell clusters.
- (E) T cell cluster genes comparing tgXist male high disease and WT female with WT male. Pristane-treated mouse groups shown: tgXist male, disease high (n = 4); tgXist male, disease low (n = 4); wild-type male (n = 3); and wild-type female (n = 2). Significance was calculated using the Wilcoxon rank-sum test.

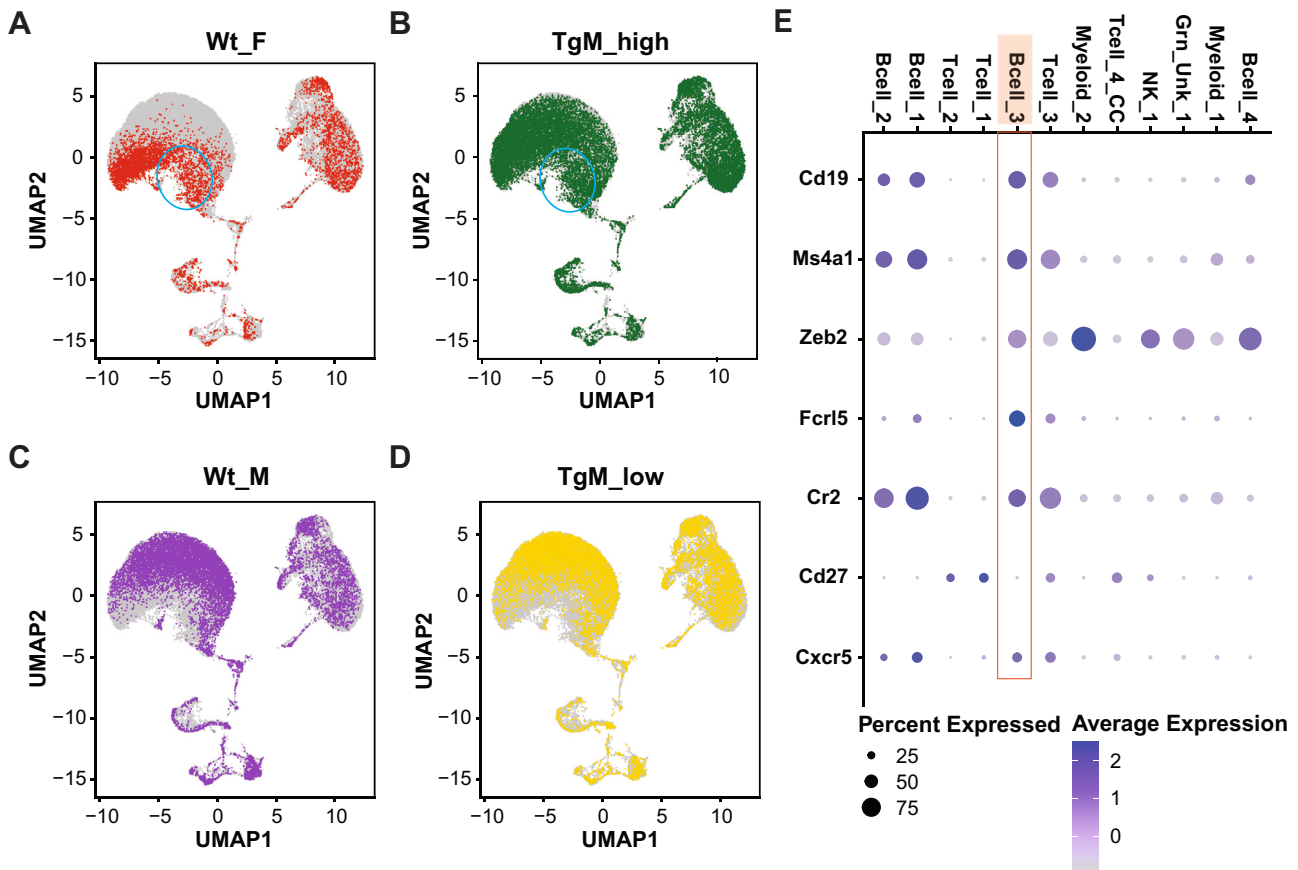


**Figure S7. Distribution of pristane-treated mouse cohorts and atypical B cells, related to Figure 5**

(A–D) UMAP distribution of cells from (A) WT female, (B) tgXist male high disease, (C) WT male, and (D) tgXist male low disease. Blue circles indicate shared overlapping regions in WT female and tgXist male high disease pristane-treated mouse groups corresponding to Bcell\_3.

(E) Dot plot of atypical B cell marker expression in gene expression clusters. Pristane-treated mouse groups shown: tgXist male, disease high (n = 4); tgXist male, disease low (n = 4); wild-type male (n = 3); and wild-type female (n = 2).